

RESEARCH ARTICLE

Spatial and temporal inhibition of FGFR2b ligands reveals continuous requirements and novel targets in mouse inner ear morphogenesis

Lisa D. Urness^{1,*}, Xiaofen Wang^{1,*}, Huy Doan^{1,*}, Nathan Shumway¹, C. Albert Noyes¹, Edgar Gutierrez-Magana¹, Ree Lu¹ and Suzanne L. Mansour^{1,2,‡}

ABSTRACT

Morphogenesis of the inner ear epithelium requires coordinated deployment of several signaling pathways, and disruptions cause abnormalities of hearing and/or balance. The FGFR2b ligands FGF3 and FGF10 are expressed throughout otic development and are required individually for normal morphogenesis, but their prior and redundant roles in otic placode induction complicates investigation of subsequent combinatorial functions in morphogenesis. To interrogate these roles and identify new effectors of FGF3 and FGF10 signaling at the earliest stages of otic morphogenesis, we used conditional gene ablation after otic placode induction, and temporal inhibition of signaling with a secreted, dominant-negative FGFR2b ectodomain. We show that both ligands are required continuously after otocyst formation for maintenance of otic neuroblasts and for patterning and proliferation of the epithelium, leading to normal morphogenesis of both the cochlear and vestibular domains. Furthermore, the first genome-wide identification of proximal targets of FGFR2b signaling in the early otocyst reveals novel candidate genes for inner ear development and function.

KEY WORDS: Otocyst, Conditional mutant, Ligand trap, RNA-Seq

INTRODUCTION

The membranous labyrinth of the mammalian inner ear is one of the most complex examples of organ morphogenesis. An unremarkable patch of cranial ectoderm is transformed into a structurally intricate sensory apparatus with two functionally distinct compartments: the ventral cochlea and the dorsal vestibular system, responsible for the perception of sound and acceleration, respectively. Within these compartments an exquisitely patterned array of sensory, non-sensory and supporting cell types are poised to transduce auditory and vestibular stimuli through sensory ganglia to the brain. Proper morphogenesis of the labyrinth is essential for normal auditory and vestibular function as indicated by imaging studies of hearing loss patients (Kimura et al., 2018; Sennaroglu and Bajin, 2017). In light of the advent of cochlear implantation to treat hearing loss in cases of inner ear malformation (Isaiah et al., 2017), elucidating the signals governing otic morphogenesis and appreciation of the

spectrum of labyrinthine morphogenetic defects are necessary to advance treatment.

Amniote inner ear development initiates during neurulation when hindbrain proximal ectoderm is induced to thicken, forming the otic placode, the source of both the otic epithelium and the neurons of its sensory ganglia. Next, the placode invaginates, forming a cup that deepens and delaminates neuroblasts, before detaching from the overlying ectoderm to form a spherical vesicle, the otocyst, which at embryonic day (E) 9.5 in mouse is already patterned along the three anatomical axes. Otocyst morphogenesis initiates with dorsomedial budding to form the endolymphatic duct and sac (EDS) anlagen. Vestibular structures initiate by sequential dorsal and lateral evaginations of the epithelium to form vertical and horizontal pouches, which are further sculpted by epithelial fusion and resorption, generating three orthogonal semicircular canals. The utricle and saccule form from anterior/central bulges, and the cochlear duct (CD) emerges as a ventral outgrowth. In mice, it undergoes progressive ventral extension and coiling, reaching 1.75 turns by E15.5, when gross morphogenesis is largely complete (Morsli et al., 1998; Sajan et al., 2007). Cell-type differentiation and functional maturation, however, continue until well after birth (reviewed by Alsina and Whitfield, 2017; Basch et al., 2016; Whitfield, 2015; Wu and Kelley, 2012).

Signals regulating otic placode induction and early otocyst patterning emanate from surrounding tissues and are understood in some detail (Ladher, 2017), but by otocyst stages intrinsic signals are also produced and their roles in driving region-specific morphogenesis are less well understood. Extrinsic signals regulating dorsal morphogenesis include hindbrain WNTs and BMPs. SHH secreted from the ventral hindbrain and notochord initiates ventral morphogenesis. Crosstalk between these signals involves regulation of key region-specific transcription factors (Ohta and Schoenwolf, 2018). FGF signaling is also crucial for otic development, and functions at multiple stages. A cascade of FGFs from endoderm, mesoderm and hindbrain is required for otic placode induction (Alvarez et al., 2003; Ladher et al., 2005; Wright and Mansour, 2003a; Zelarayan et al., 2007). In particular, *Fgf3* and *Fgf10*, encoding ligands that signal through FGF receptor isoforms FGFR1b and FGFR2b (Zhang et al., 2006), are required redundantly for otic placode induction, such that germline double null mutants (F3KO;F10KO) have no inner ear (Alvarez et al., 2003; Wright and Mansour, 2003a). Applications of FGFs and FGFR inhibitors to chick embryos revealed profound influences of FGFs on otic morphogenesis (Chang et al., 2004) and studies of individual mouse mutants revealed roles for *Fgf3* and *Fgf10* in morphogenesis. Mice lacking *Fgf3* (F3KO) fail with variable penetrance and expressivity to form an EDS, and consequently have variable morphogenesis and dysfunction of both the cochlea and vestibule

¹Department of Human Genetics, University of Utah, Salt Lake City, UT 84112-5330, USA. ²Department of Neurobiology and Anatomy, University of Utah, Salt Lake City, UT 84112-5330, USA.

*These authors contributed equally to this work

‡Author for correspondence (suzi.mansour@genetics.utah.edu)

© S.L.M., 0000-0001-9040-302X

(Hatch et al., 2007; Mansour et al., 1993). Mice lacking *Fgf10* (F10KO) have no posterior semicircular canals (PSCCs), and show milder deformations of the anterior and lateral canals. *Fgf10* heterozygotes also exhibit PSCC reductions or agenesis (Pauley et al., 2003; Urness et al., 2015). The F10KO CD is also affected, being shorter and narrower than that of heterozygous or wild-type mice owing to loss of non-contiguous non-sensory domains (Urness et al., 2015). *Fgf2b* null mutants form otocysts (Pirvola et al., 2000); however, they develop with severe cochlear and vestibular dysmorphology, suggesting that *Fgf3* and *Fgf10* could have additional and combinatorial roles during morphogenesis.

Here, we define the expression of *Fgf3* and *Fgf10* in the developing mouse otic epithelium and ganglion, and interrogate their functions after otic placode induction. We employ two complementary genetic strategies: otic placode lineage-restricted gene ablation and timed induction of a soluble dominant-negative FGFR2b ectodomain that acts rapidly as an extracellular ligand trap to block signaling. Together, our data show that *Fgf3* and *Fgf10* are not required in the placode lineage for otocyst formation, but are required subsequently for otocyst patterning, neuroblast maintenance, epithelial proliferation and both vestibular and cochlear morphogenesis. Furthermore, the first differential RNA-Seq analyses of otocysts revealed FGFR2b signaling targets that define novel candidates for involvement in otic morphogenesis and function.

RESULTS

***Fgf3* and *Fgf10* are expressed dynamically during otocyst and ganglion formation, and cochlear morphogenesis**

To determine *Fgf3* and *Fgf10* expression during otocyst formation and cochlear morphogenesis, we used RNA *in situ* hybridization (ISH). Before E9.0, both genes were exclusively periotic (data not shown). Consistent with previous studies (Schimmang, 2007; Wright and Mansour, 2003b), *Fgf3* and *Fgf10* transcripts were non-overlapping at the otic cup stage, with *Fgf3* expressed in hindbrain adjacent to the cup, and *Fgf10* expressed in the cup itself, exclusive of the dorsal and lateral-most regions (Fig. 1A,B). Once the otocyst closed, *Fgf3* was diminished in the hindbrain and was first seen in the ventrolateral otocyst and in the forming otic ganglion, whereas *Fgf10* was expressed in the ventral and medial otocyst (Fig. 1C,D). By E10.25–E11.25, *Fgf3* was confined to the ventrolateral otocyst. At this stage, *Fgf10* overlapped with and was more extensively expressed in the ventral otocyst than was *Fgf3*, and also began to be expressed strongly in the ganglion (Fig. 1E–H).

We confirmed overlap of *Fgf3* and *Fgf10* in the developing vestibular sensory tissues, with *Fgf10* expression much stronger than *Fgf3* (data not shown; see Pauley et al., 2003; Pirvola et al., 2000). Focusing on the developing CD, from E12.5–E16.5, we found *Fgf3* in a progressively limited portion of the CD that appeared by E16.5 to flank the developing sensory organ of Corti. *Fgf10* continued expression in a broader domain than *Fgf3*, resolving to Kölliker's organ by E16.5, and was maintained at high levels in the cochlear ganglion (Fig. 1I–P). These observations suggested that *Fgf3* and *Fgf10* could have combinatorial roles in morphogenesis and ganglion development.

Epithelial *Fgf3* and *Fgf10* are not required for otocyst formation, but both are required for vestibular and cochlear morphogenesis

Because F3KO;F10KO embryos lack otocysts, we disrupted these genes individually and combinatorially after otic placode induction using Tg(*Pax2-Cre*), which is active in the otic placode lineage

starting at E8.5 (Fig. 2A; Ohyama and Groves, 2004) and recombines in both the epithelium and ganglion (Fig. 2B,C). We evaluated gross otic morphogenesis by paintfilling at E15.5 and CD development by histology at E18.5. In contrast to the variable F3KO otic phenotypes (Hatch et al., 2007; Mansour et al., 1993), disruption of *Fgf3* in the *Pax2-Cre* lineage (F3cKO) had no effect on otic morphogenesis or on CD histology (Fig. 2D–E'). Indeed, F3cKO animals survived in the expected numbers and had normal auditory thresholds and motor behavior (data not shown). In contrast, F10cKO ears showed both vestibular and cochlear abnormalities, including reduction or loss of the PSCC and variable CD shortening and narrowing, the latter reflecting loss of Reissner's membrane (Fig. 2F–G'). These abnormalities were similar to those of F10KO ears (Urness et al., 2015) and, indeed, immunostaining of E18.5 F10cKO CDs was similar to F10KO CDs (data not shown). Notably, *Fgf10*^{−/c} *Cre*-negative ears had mild PSCC shortening, but CD defects appeared only in F10cKO ears (Fig. 2F,F').

Next, we evaluated morphogenesis after varying *Fgf3* and *Fgf10* dosage. At E9.5, all embryos had otocysts starting to develop an endolymphatic duct, showing that otic placode induction occurred normally, even in the absence of both *Fgf* genes (Fig. 2H–K'). However, E15.5 ears showed genotype-dependent morphologic defects (Fig. 2L–O'). Even *Cre*-negative ears had PSCC defects when heterozygous for *Fgf10* (Fig. 2N,O). Not surprisingly, all *Cre*-positive ears had reduced or absent PSCCs, as *Fgf10* is at least heterozygous in those cases (Fig. 2L',M',N',O'). Ears were classified according to the scheme used for *Fgf10* mutants (Urness et al., 2015) and formed a phenotypic spectrum of increasing severity (Table S1). Most F3cHet;F10cHet ears showed only mild PSCC reductions (Fig. 2L'), whereas most F3cKO;F10cHet ears lacked a PSCC (Fig. 2M'). However, most F3cHet;F10cKO ears had an unfused vestibular pouch, reductions in the saccule and utricle, and more extensive shortening and narrowing of the CD (Fig. 2N') than in F10cKO ears (Fig. 2F'). Only the EDS appeared normal. The distribution of F3cHet;F10cKO phenotypes was significantly more severe than that of F10cKO phenotypes ($P < 10^{-4}$; Table S1). However, limited cochlear marker gene analyses of E18.5 F3cHet;F10cKO ears did not reveal any exacerbation of changes seen previously in F10KO ears (data not shown; see Urness et al., 2015) and the apparent narrowing of the CD was not significant (Fig. S1). Strikingly, conditional disruption of both *Fgf3* and *Fgf10* blocked both vestibular and cochlear development, leaving only a small spherical vesicle (Fig. 2O'). F3cHet;F10cHet and F3cKO;F10cHet CD histology (Fig. 2P–Q') was indistinguishable from that of F3cKO (Fig. 2E,E'), whereas F3cHet;F10cKO CDs were very narrow and lacked Reissner's membrane (Fig. 2R,R'), similar to those of F10cKO (Fig. 2G,G') and F10KO CDs (Urness et al., 2015). The F3cKO;F10cKO 'ear' had an epithelium comprising a thin, non-sensory region and a thickened vestibular-like sensory region. Most notably, these mutants showed no evidence of cochlear or vestibular neurons (Fig. 2S,S'). These data show that both *Fgf3* and *Fgf10* are required in the *Pax2-Cre* lineage, not only for vestibular morphogenesis, but also for cochlear morphogenesis and otic gangliogenesis, with the effect of *Fgf3* being revealed only in the absence of *Fgf10*.

***Fgf3* and *Fgf10* are not required in the *Pax2-Cre* lineage for early otocyst proliferation, but are required for otocyst patterning and maintenance of otic neuroblasts**

As F3cKO;F10cKO embryos ultimately develop very small otic vesicles, and this was first apparent at E10.5–E11.5, we quantified

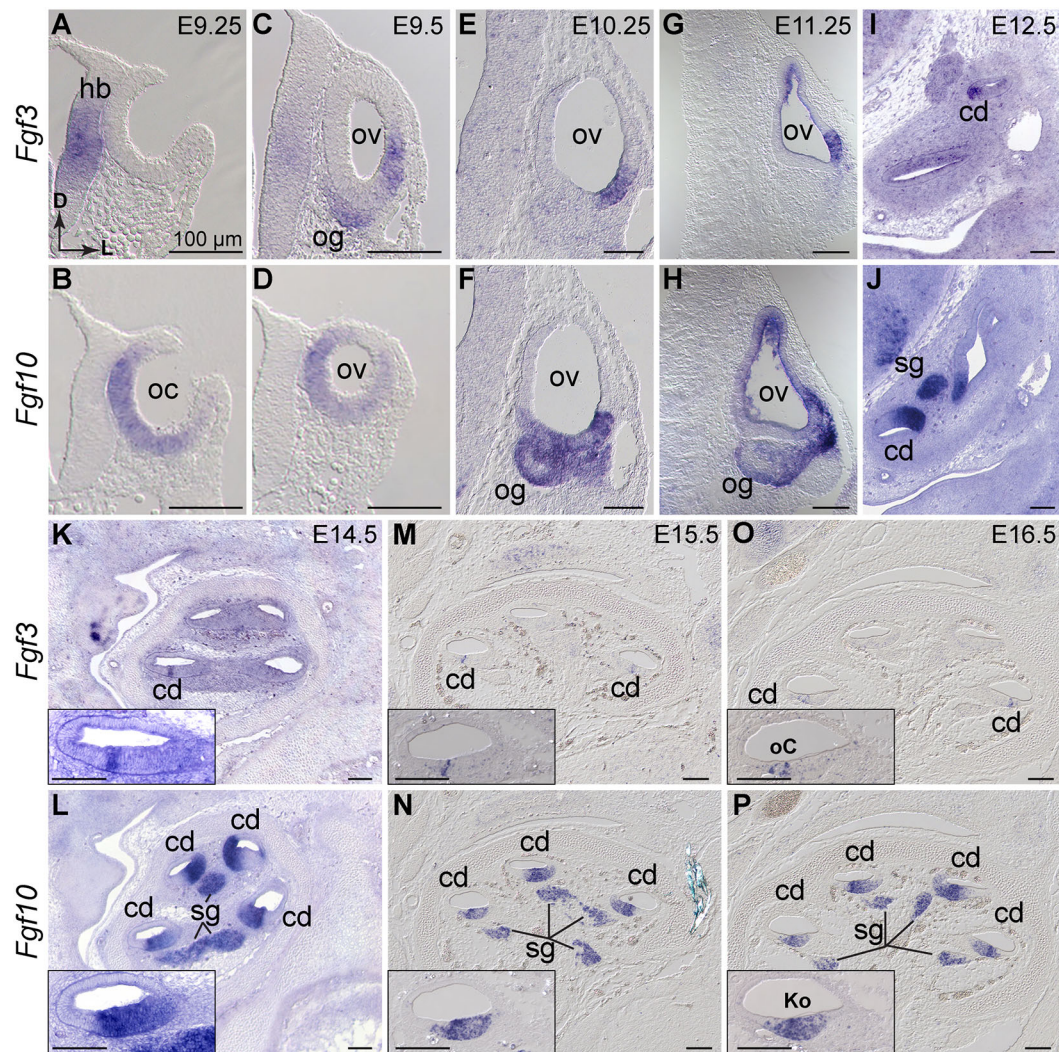


Fig. 1. *Fgf3* and *Fgf10* are expressed throughout otocyst formation and cochlear morphogenesis. (A-P) ISH of *Fgf3* and *Fgf10* probes to wild-type otic cup (A,B), otic vesicle (C-H) and cochlear duct (I-P). Probes are indicated to the left and developmental ages at the top right of each paired column. (A-J) Transverse orientation, directional arrows in A apply to all. (K-P) Sagittal orientation with cochlear apex at the top. Insets show basal-most cochlear turn. cd, cochlear duct; D, dorsal; hb, hindbrain; Ko, Kölliker's organ; L, lateral; oc, organ of Corti; og, otic ganglion; ov, otic vesicle; sg, spiral ganglion. Scale bars: 100 μ m.

mitotic cells in E10.5 otocyst sections by calculating the number of phosphohistoneH3 (pHH3)-positive cells per otic epithelial area. The difference between control and F3cKO;F10cKO vesicles, however, was not significant (Fig. S2A-C); cleaved caspase 3, a measure of dying cells, was similarly unaffected (Fig. S2C'). This may be because hindbrain *Fgf3* (Fig. 1A,C), which is unaffected by *Pax2-Cre* and is required to form a normally sized otocyst (Fig. S2D-G'), is sufficient to promote otocyst proliferation and survival through E10.5.

To assess otocyst patterning in conditional mutants, we conducted whole-mount ISH of E9.5-E11.5 samples using probes for regionally expressed genes that are known targets of FGF3 and/or FGF10 signaling and/or are required for morphogenesis. To manage the number of samples analyzed, we omitted single conditional mutants and used only a single *Cre*-negative genotype (*Fgf3*^{-/-};*Fgf10*^{-/-}). At E9.5, most genes tested, as exemplified by *Sox9*, were unaffected even in F3cKO;F10cKO ears (Fig. 3A). Other genes unaffected by loss of both *Fgf3* and *Fgf10* alleles at this stage included *Dusp6*, *Spry1*, *Foxg1*, *Has2*, *Gbx2*, *Hmx3*, *Sox2* and *Pax2* (data not shown), all of which are lost in F3KO;F10KO ears by

otic placode stages (Alvarez et al., 2003; Urness et al., 2010; Wright and Mansour, 2003a). However, the common FGF signaling target, *Etv5*, which has distinct ventromedial and dorsolateral domains in E9.5 control otocysts, showed differential localization in conditional mutants with only a single *Fgf3* or *Fgf10* allele remaining, and expression was entirely absent from F3cKO;F10cKO ears (Fig. 3B), demonstrating that epithelial FGF3/FGF10 signaling was disrupted within 24 h of CRE activation. The only other gene affected at E9.5 was *Tbx1*, which had dorsolateral and posteroventral otocyst domains in all genotypes except F3cKO;F10cKO, which lost the dorsolateral domain (Fig. 3C). By E10.5, the dorsolateral *Tbx1* domain was lost from both F3cHet;F10cKO and F3cKO;F10cKO otocysts (Fig. 3D).

At E10.5, expression of several other genes was still unaffected, as exemplified by *Gbx2* (Fig. 3E), which is required for vestibular morphogenesis (Lin et al., 2005) and is downregulated at this stage in F3KO mutants (Hatch et al., 2007). Other genes unaffected at E10.5 included *Hmx3*, *Spry2*, *Gli1*, *Id1* and *Lfng* (data not shown). In contrast, *Sox2*, *Foxg1* and *Bmp4*, which are primarily lateral at E10.5, were extinguished in F3cKO;F10cKO ears (Fig. 3F-H).

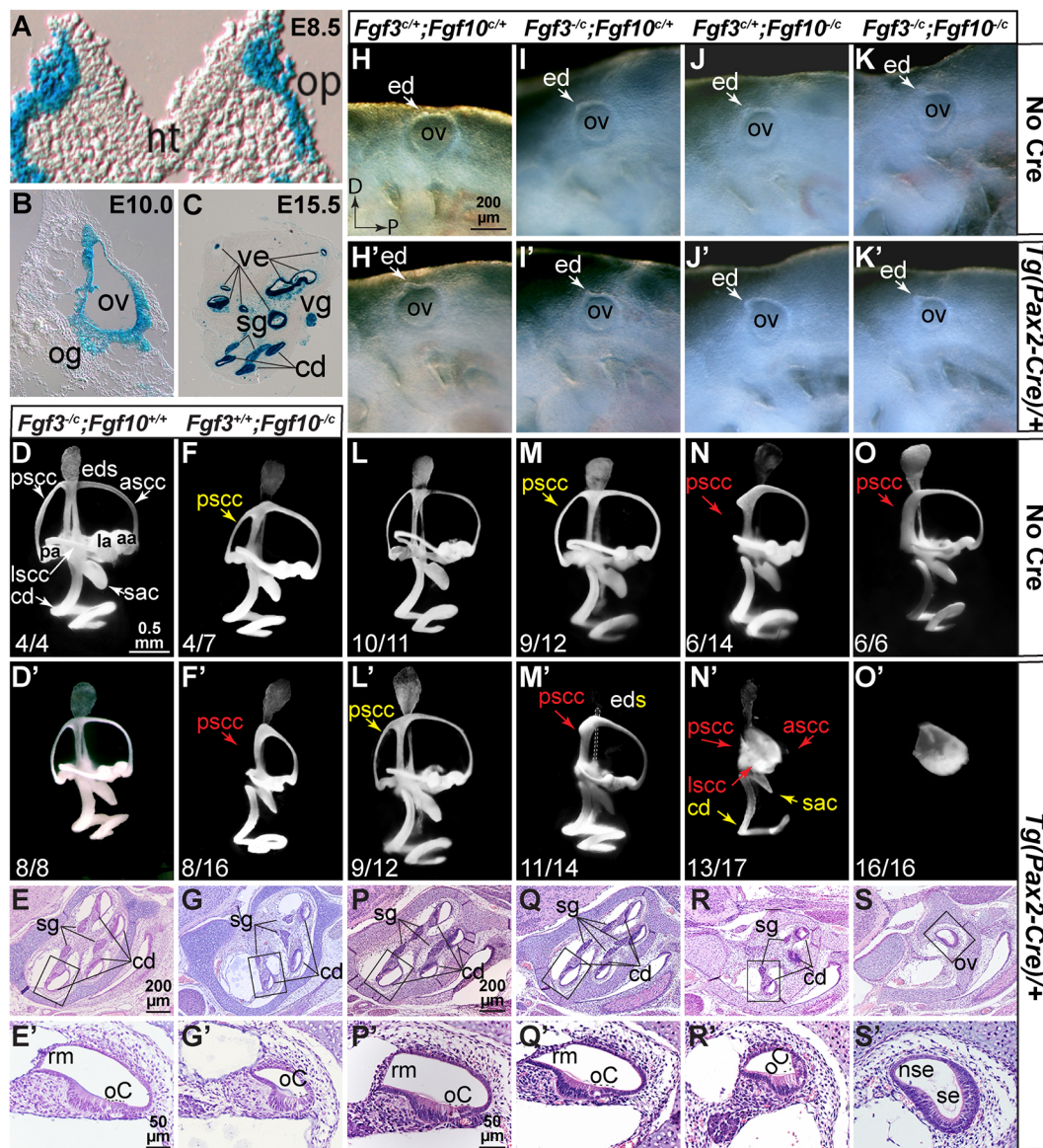


Fig. 2. *Fgf3* and *Fgf10* are not required in the *Pax2-Cre* lineage for otocyst formation, but both are required subsequently for vestibular and cochlear morphogenesis. (A-C) *Pax2-Cre* otic lineage (blue) at indicated stages. (H-K') E9.5 left otocysts showing normal development. (D-F',L-O') E15.5 paintfilled ears, right lateral views of most common phenotype (enumerated in Table S1). (E-G',P-S') E18.5 Hematoxylin and Eosin-stained sagittal cochlear sections. Boxed regions are enlarged in E',G',P'-S'. Fgf genotypes are shown above each column and *Cre* status indicated to the right. Yellow text indicates apparent length reductions, red text indicates expected positions of missing structures. aa, anterior ampulla; ascc, anterior semicircular canal; cd, cochlear duct; ed, endolymphatic duct; eds, endolymphatic duct/sac; la, lateral ampulla; lscc, lateral semicircular canal; nt, neural tube; nse, non-sensory epithelium; oC, organ of Corti; og, otic ganglion; op, otic placode; ov, otic vesicle; pa, posterior ampulla; pscc, posterior semicircular canal; rm, Reissner's membrane; sac, saccule; se, sensory-like epithelium; sg, spiral ganglion; ve, vestibular epithelium; vg, vestibular ganglion. Scale bar in H applies to H-K'; in D to D-F',L'-O'; in E, to E,G; in E' to E',G'; in P to P-S; and in P' to P'-S'.

Other genes lost at E10.5 included *Dusp6*, *Etv5*, *Etv4* and *Spry2* (data not shown), all of which are transcriptional targets of FGF signaling. Curiously, we found that *Pax2*, which at E10.5 is normally expressed medially, was unchanged in all otocysts except F3cKO/F10cKO, where it was expanded (Fig. 3I). By E11.5 the only tested genes still unaffected in F3cKO/F10cKO otocysts were *Gli1*, *Hmx3*, *Lfng* and *Id1* (data not shown), so these are unlikely to be targets of FGF3/FGF10 signaling in the otocyst.

To assess the otic ganglion, we assayed *Neurog1* and its target, *Neurod1*, at both E9.5 and E10.5. At E9.5, all genotypes exhibited similar expression in a ventrolateral epithelial domain and in delaminating neuroblasts (Fig. 3J,L). In contrast, at E10.5 *Neurog1* was strongly reduced and *Neurod1* was virtually eliminated from the

otic epithelium, and otic ganglion development was suppressed specifically in F3cKO/F10cKO otocysts (Fig. 3K,M). These data show that epithelial/ganglion expression of *Fgf3* and *Fgf10* are required for aspects of gene expression driving otic morphogenesis, particularly in lateral regions, and that they are also required for otic ganglion formation.

Doxycycline induction of a secreted FGFR2b ectodomain phenocopies F3KO;F10KO mutants

FGF3 and FGF10 bind to and signal through 'b'-type FGF receptors (FGFR2b>FGFR1b; Zhang et al., 2006). To enable simultaneous and inducible inhibition of their signaling activity at any stage, we employed two alleles that together enable doxycycline (DOX)-

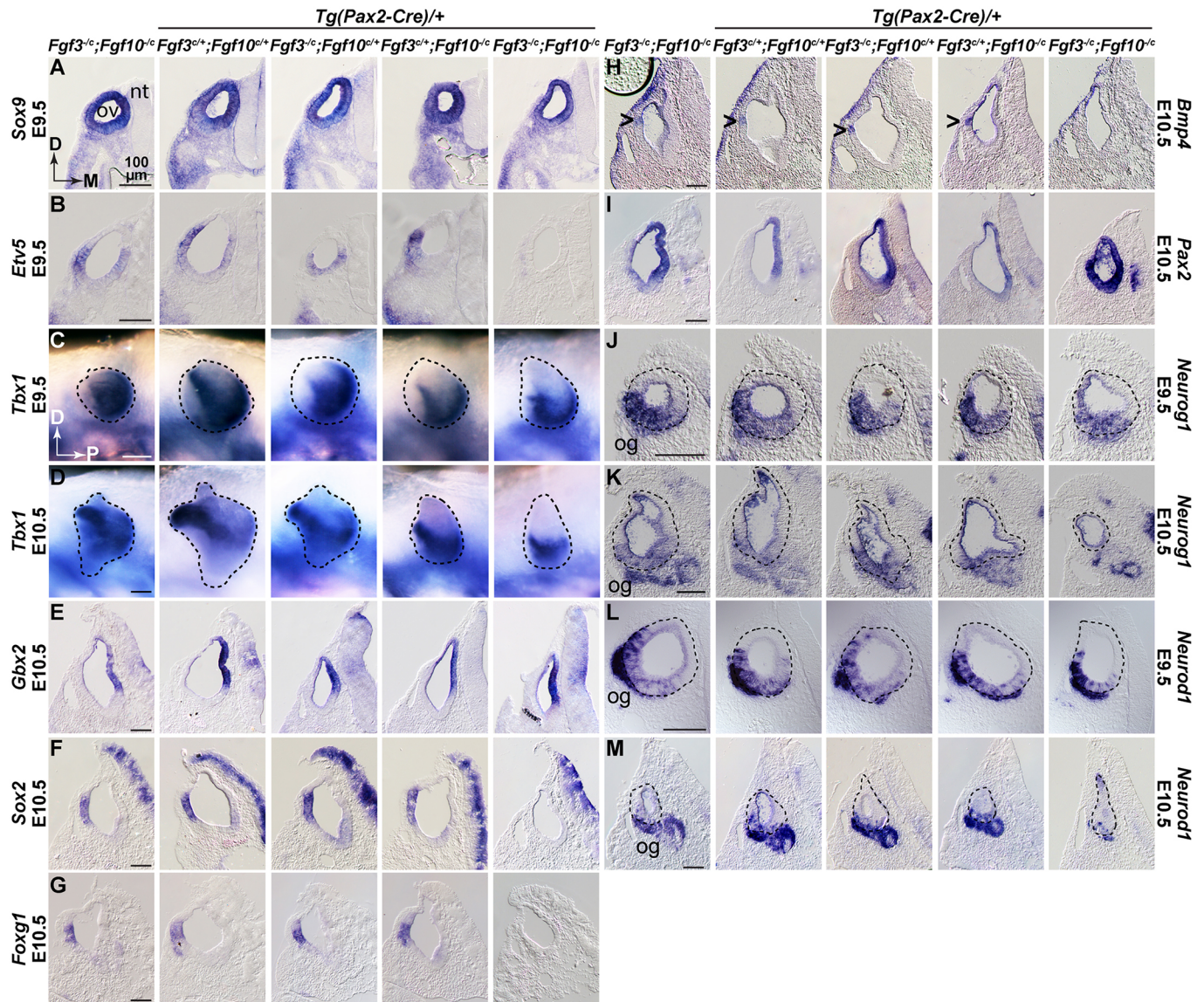


Fig. 3. *Fgf3* and *Fgf10* are required in the *Pax2-Cre* lineage for otocyst patterning and maintenance of otic neuroblasts. (A–M) Transverse sections through the ov (A,B,E–M), or whole mounts (C,D), of embryos subjected to ISH. Probes and developmental stages are indicated aside each row. Genotypes are shown atop each column. Scale bars (100 μ m) apply to each probe/stage group. Arrowheads in H indicate *Bmp4* expression. Directional arrows in A and C apply to all sections and whole-mounts, respectively. D, dorsal; M, medial; nt, neural tube; og, otic ganglion; ov, otic vesicle; P, posterior.

inducible expression of a secreted, dominant-negative form of FGFR2b (dnFGFR2b), which serves as a ligand trap. *Rosa26^{rtTA}* drives ubiquitous expression of the reverse tetracycline transactivator (Belteki et al., 2005) and *Tg(tetO-dnFgfr2b)* encodes a tetO-regulated and secreted FGFR2b ectodomain (Hokuto et al., 2003). This system is validated for temporally controlled inhibition of FGFR2b/1b-dependent mammary gland, tooth, limb and lung development (Al Alam et al., 2015; Danopoulos et al., 2013; Parsa et al., 2010; Parsa et al., 2008).

To validate this system for inner ear studies, we fed DOX-containing chow (DOX-chow) to pregnant females from E5.5–E10.5 and observed gross embryonic phenotypes. *Rosa26^{rtTA/+}* (control) embryos appeared normal, but *Rosa26^{rtTA/+};Tg(tetO-dnFgfr2b)/+* (experimental) embryos had a short curly tail, lacked limb buds and had tiny otic vesicles (Fig. 4A,B), phenocopying F3KO;F10KO mutants. Experimental embryos exposed to DOX from E5.5 or E6.5 to E11.5 showed only an otic remnant (Fig. S3)

and did not exhibit mid-hindbrain phenotypes characteristic of inhibition of ligands such as FGF8 and FGF17 that signal through γ -type FGFRs (Chi et al., 2003; Sato and Joyner, 2009; Xu et al., 2000).

Secreted dnFGFR2b acts rapidly to inhibit signaling by FGFR2b ligands

To determine the timing of signaling inhibition, we initiated dnFGFR2b expression by injecting DOX at different stages, providing DOX-chow for various intervals, and assaying for *Etv5* expression by ISH. After only 4 h of DOX starting at E9.5, *Tg(tetO-dnFgfr2b)/+* embryos showed robust *Etv5* expression in numerous sites of FGF signaling, including throughout most of the otic vesicle (Fig. 4C,C'). In contrast, experimental embryos retained expression of *Etv5* at many sites, but lacked otic *Etv5* (Fig. 4D,D'). In addition, 6 h of DOX starting at E8.25 nearly ablated *Etv5* throughout experimental embryos, including in the otic cup (Fig. S4A–B') and 4 h of DOX starting at E10.25 significantly

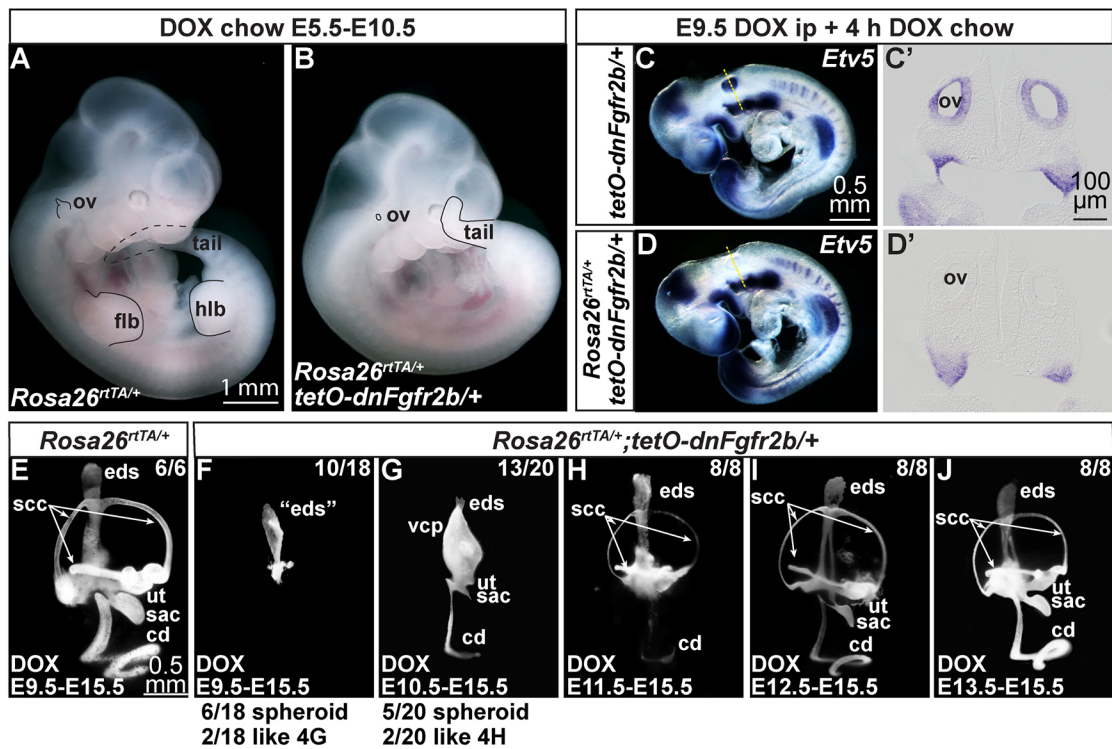


Fig. 4. Induction of dnFGFR2b phenocopies F3KO;F10KO mutants and acts rapidly, revealing continuous requirements for FGFR2b ligands in otic morphogenesis. (A,B) E10.5 control and experimental embryos exposed to DOX from E5.5 to E10.5. Affected structures are outlined in black; dashed lines indicate regions behind the embryo. Scale bar in A applies to B. (C-D') E9.5 control and experimental embryos exposed to DOX for 4 h and hybridized with *Etv5*. Dashed lines in C,D indicate transverse section planes for C',D'. Scale bars in panels C,C' apply to D,D'. (E-J) E15.5 paintfilled inner ears from embryos exposed to DOX for the interval indicated at the bottom of each panel. Number of ears with the phenotype shown is indicated. Additional phenotypes listed below. Scale bar in E applies to F-J. cd, cochlear duct; eds, endolymphatic duct/sac; flb, forelimb bud; hlb, hindlimb bud; ov, otic vesicle; sac, saccule; scc, semicircular canal; ut, utricle; vcp, vertical canal pouch.

downregulated *Etv5* in the dorsolateral quadrant of the otic vesicle (Fig. S4C-D'). Thus, inhibition of FGFR2b ligands has a rapid onset in otic tissue, consistent with studies of dnFGFR2b induction in the limb (Danopoulos et al., 2013).

FGFR2b ligands are required continuously for otic morphogenesis

Next, we asked when FGFR2b ligands are required for otocyst morphogenesis. We started dnFGFR2b expression on different days of development and sustained the induction through E15.5, when inner ears were paintfilled. We compared *Rosa26^{rtTA/+}* control to experimental samples. E8.5-E15.5 DOX exposure completely inhibited inner ear development ($n=6/6$; data not shown). E9.5-E15.5 DOX exposure had no effect on controls (Fig. 4E), but experimental ears showed three distinct phenotypes: six had a small spheroid chamber similar to that of F3cKO;F10cKO samples (Fig. 2O'), ten had a structure resembling an EDS (Fig. 4F) and two resembled the majority of the E10.5-E15.5 group (Fig. 4G). DOX from E10.5-E15.5 also caused three phenotypic variants: five had a spheroid chamber, 13 had a vertical canal pouch, but no SSCs, a small saccule and utricle, and a dramatically shortened and narrowed CD (Fig. 4G), resembling the most strongly affected F10KO mutants (Urness et al., 2015), and two resembled the E11.5-E15.5 treatment group (Fig. 4H). DOX from E11.5-E15.5 caused consistent phenotypes: all ears had narrowed SSCs, reductions of the utricle and saccule, and a narrow and short CD (Fig. 4H). DOX from E12.5-E15.5 also caused consistent phenotypes: all ears had narrow SSCs, somewhat reduced utricles and saccules, and a narrow CD that nevertheless appeared normally elongated and coiled

(Fig. 4I). Even experimental ears exposed to DOX from only E13.5-E15.5 had consistently narrow SSCs, but the rest of the inner ear appeared grossly normal (Fig. 4J). These data show that FGFR2b ligands are required continuously during otic morphogenesis.

Transient activation of dnFGFR2b reveals critical periods for FGFR2b ligands in otic morphogenesis

To determine intervals for FGFR2b ligand requirements in particular events of otic morphogenesis, we treated pregnant dams with different DOX pulses and examined E15.5 inner ears by paintfilling. As expected, all control ears, regardless of DOX exposure had normal morphology (Fig. 5A,E,G,K,M,Q). Experimental ears, however, showed exposure time-dependent abnormalities. A 4-h DOX exposure starting at 09.00 on E8.5 (termed E8.25) caused mild PSSC reductions in three ears, two of which also featured a truncated EDS and thickened CD (Fig. 5B), but had no effect on the remaining ears (not shown). 6-h or 24-h exposures had increasingly severe consequences. Most of the 6-h group and some of the 24-h group lacked an EDS (Fig. 5C',D). The majority of 24-h exposures blocked most development of the otocyst, leaving a small vesicle (Fig. 5D') or no ear tissue (not shown). By delaying DOX administration to 21.00 on E8.5 (called E8.75) all experimental samples with any ear tissue ($n=17/32$) showed at least an EDS and most of these ($n=12/32$) had a central (vestibular) segment and a linear CD (Fig. 5F,F'). A 2-h DOX pulse starting at 09.00 on E9.5 (called E9.25) had no effect on morphogenesis (data not shown), but 4- or 6-h exposures consistently caused only PSSC defects (Fig. 5H-I'). The 24-h exposures allowed EDS-like outgrowth, but consistently blocked

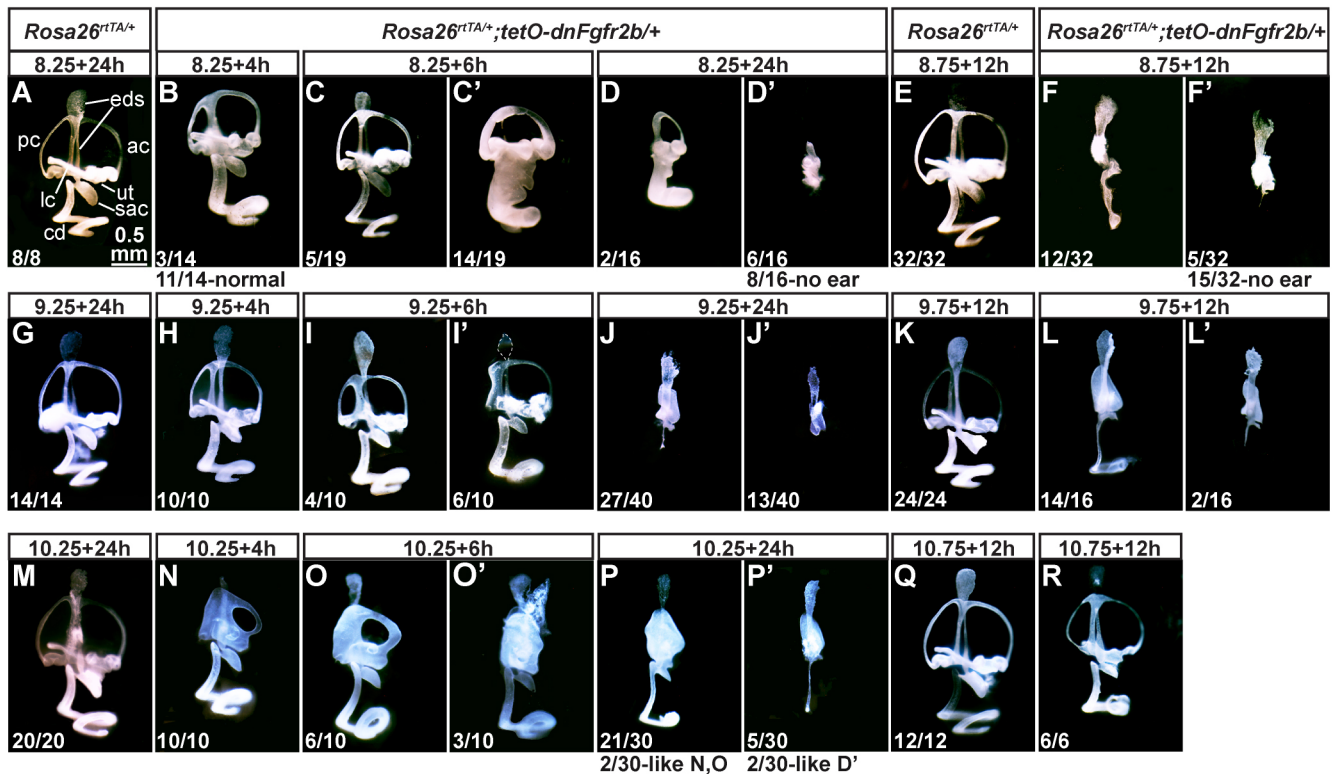


Fig. 5. Transient activation of dnFGFR2b reveals critical periods for FGFR2b ligands in otic morphogenesis. (A-R) Paintfilled ears from control and experimental embryos with genotypes indicated above. DOX was provided to pregnant dams at E8.25 (A-D'), E8.75 (E-F'), E9.25 (G-J'), E9.75 (K-L'), E10.25 (M-P') or E10.75 (Q,R) for the hours indicated above each panel. The number of ears from each treatment showing the same phenotype is indicated at the lower left. Alternate phenotypes are enumerated below. Scale bar in A applies to all panels. ac, anterior canal; cd, cochlear duct; eds, endolymphatic duct/sac; lc, lateral canal; pc, posterior canal; ut, utricle.

most vestibular and cochlear outgrowth (Fig. 5J,J'). 12-h DOX exposures starting at 21.00 on E9.5 permitted EDS outgrowth and formation of at least a vertical canal pouch, but no SCC formation. In addition, the CD was short and narrow ($n=14/16$) or not present ($n=2/16$; Fig. 5L,L'). 4- or 6-h DOX exposures starting at 09.00 on E10.5 (termed E10.25) consistently blocked normal PSCC formation and the 6-h exposure sometimes affected the anterior semicircular canal (ASCC), but had virtually no effect on development of the utricle, saccule or CD (Fig. 5N-O') until the exposure reached 24 h (Fig. 5P,P'). By starting DOX at 21.00 on E10.5 (termed E10.75), the most severe defects were avoided; nevertheless, the SCCs appeared thin, the utricle and saccule were reduced and the CD was short (Fig. 5R). In summary, we found that the earlier DOX was started and the longer it was present, the more severe were the morphogenesis defects. Furthermore, some of the DOX pulses gave such consistent outcomes that it seemed possible to identify acute epithelial transcriptional targets of FGFR2b ligands mediating particular morphogenetic events.

RNA-Seq reveals transcriptional targets of FGFR2b ligands during early otic morphogenesis

To identify transcriptional targets of FGFR2b ligands during early otocyst morphogenesis, when they are required for both vestibular and cochlear outgrowth, we chose three overlapping DOX exposures (Fig. 6A) that gave similar morphogenesis outcomes: E9.75+12 h (Seq1, Fig. 5L,L'), E10.25+24 h (Seq2, Fig. 5P,P') and E9.25+24 h (Seq3, Fig. 5J,J'). Embryonic otocysts were microdissected, cleaned of mesenchyme (Fig. 6B), and pooled into control and experimental groups from each female. RNA was

isolated, processed for RNA-Seq and analyzed for differential expression under both unpaired (genotype only) and paired (genotype and litter) statistical models.

Differentially expressed genes with an adjusted (adj) $P < 0.05$ in each paired dataset were visualized with volcano plots (Fig. 6C; Fig. S5). In all three datasets, the maximum fold-changes were relatively modest, perhaps reflecting the short periods of inhibition, but for many genes the differences were highly significant. *Fgfr2* and *Ighg1* were among the most differentially expressed Seq1 genes (5.3-fold and 633-fold induced, respectively, but *Ighg1* was omitted from the plot for legibility; Fig. 6C). Inspection of *Fgfr2* reads showed upregulation was due to *Fgfr2b* splice isoform expression specifically in transgene-containing samples. *Ighg1* reads were also transgene-encoded, thus validating the efficacy of the inductions. Excluding *Fgfr2* and *Ighg1*, there were 968 genes >1.5 -fold upregulated and 631 genes >1.5 -fold downregulated (adj $P < 0.05$) in experimental otocyst RNA. Significantly downregulated genes included well-known transcriptional targets of FGF signaling, *Etv1*, *Etv4*, *Etv5*, *Dusp6*, *Spry2* and *Spry1* (Fig. 6C; listed in Table S4, sheet 1). Similar results were obtained for RNA-Seq2 and RNA-Seq3 (Fig. S4; listed in Table S4, sheet 1). To validate an FGF target gene significantly downregulated in all three datasets, we detected *Etv5* by ISH of otocyst sections. Seq1 control otocysts showed lateral and ventromedial *Etv5* expression, whereas experimental embryos did not express otocyst *Etv5* (Fig. 6D,E). Similar results were obtained with Seq3 samples (Fig. S6).

Fgfr1 sequence reads in each dataset showed no changes in level between control and experimental samples, which were similar to control levels of *Fgfr2*. Interestingly, *Fgfr1c*, considered

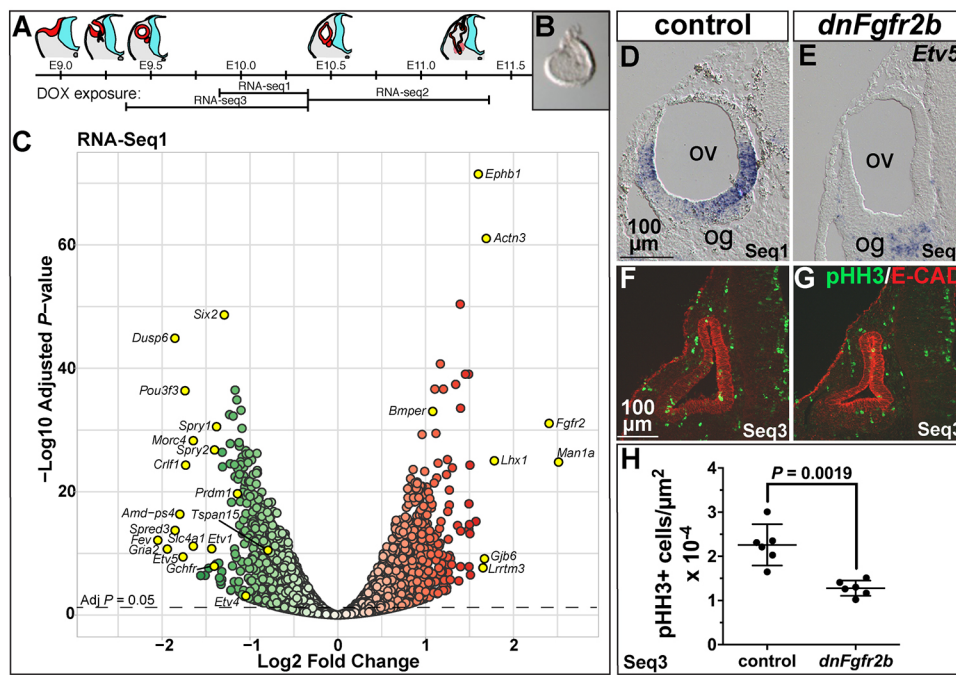


Fig. 6. Differential RNA-Seq reveals expected and novel targets of FGFR2b ligands during early otic morphogenesis and their requirement in otic epithelial proliferation. (A) Schematic of otocyst morphogenesis correlated with the three DOX exposures used for RNA-Seq. Red represents otic tissue, blue represents neural tissue. (B) Microdissected E10.25 otocyst. (C) RNA-Seq1 volcano plot showing significantly downregulated (green) and upregulated (red) genes. Significance is plotted on the y-axis and fold-change on the x-axis. Gene labels highlighted in yellow indicate fold-change >1.5, common FGF target genes, and genes pursued for ISH validation. (D,E) Transverse sections of E10.25 control and *dnFgfr2b* RNA-Seq1 otocysts hybridized with *Etv5*. (F,G) Transverse sections of E10.25 control and *dnFgfr2b* RNA-Seq3 otocysts immunostained for pHH3 (green) and E-cadherin (red). (H) Quantification of pHH3-positive cells per otic epithelial area (shown with mean and 95% c.i.) in RNA-Seq3 control and *dnFgfr2b* otocysts. Scale bars in D,F apply to E,G. og, otic ganglion; ov, otic vesicle.

mesenchymal (Pirvola et al., 2004), was the predominant splice isoform, but *Fgfr1b* was also detected. *Fgfr3* sequences were present at levels at least 20-fold below those of *Fgfr1* or *Fgfr2* in control samples and were unchanged by *dnFGFR2* induction (Table S4, sheet 1). The only FGFR2b ligand genes expressed at significant levels in control or experimental otocysts were *Fgf3* and *Fgf10* (Table S4, sheet 1), consistent with ISH surveys (Wright et al., 2003; data not shown). Interestingly, *Fgf3* was slightly, but significantly, upregulated in all three datasets. However, as *dnFGFR2b* inhibition acts at the level of protein, this is unlikely to impact the phenotypes.

FGFR2b ligands promote otocyst cell proliferation

To explore functional relationships between significantly differentially expressed genes in each dataset (either up or downregulated; $\text{adj}P < 0.05$), we used Ingenuity Pathway Analysis. In each case, the top 5 affected pathways included cell cycle and DNA damage/repair pathways [Table S4, sheet 2; $-\log(P\text{-value}) = 8\text{--}13$]. In most cases, these genes were downregulated in our datasets. In addition, we used GOrilla software to identify gene ontology terms for processes enriched in the downregulated Seq1 dataset ($\text{adj}P < 0.05$), and the results were similar (top 5 shown in Table S4, sheet 2; FDR q-values 1.55×10^{-21} – 7.84×10^{-13}). To assess proliferation directly, we quantified pHH3-positive cells per otic epithelial area in Seq3 otocyst sections and found that the mean labeling of experimental samples was reduced significantly to 57% of the control mean (Fig. 6F–H), showing that one role for FGFR2b ligands during E9.25–E10.25 is to control otic epithelial proliferation.

Signaling by FGFR2b ligands in the early otocyst represses genes that function later in otic epithelial development or hearing

Among the significantly upregulated genes in *dnFgfr2b* samples from Seq1, we noticed a gene required for hearing (*Gjb6*; Fig. 6C). Other such genes included *Cldn14*, *Tmprss3*, *Pcdh15* and *Gjb2*

(Table S4, sheet 1). To determine whether additional such genes, or those responsible for mouse hearing loss and/or cochlear development, were enriched in either the up- or downregulated genes, we conducted a gene set enrichment analysis (Subramanian et al., 2005) on all 16,232 genes detected in the Seq1 paired analysis using two partially overlapping gene lists: 95 human hereditary hearing loss genes identified by Nishio et al. (2015; rank listed in Table S4, sheet 3) and 258 mouse genes involved in inner ear development or function collated by Ohlemiller et al. (2016; rank listed in Table S4, sheet 4). Both gene sets were highly enriched in the upregulated Seq1 dataset (normalized enrichment score=2.09 for the human genes and 2.06 for the mouse genes; both nominal P -values $< 1 \times 10^{-3}$), but not in the downregulated set. Similar results were obtained with the Seq2 dataset (data not shown). Together, these analyses suggest that one role of FGFR2b ligands at this early stage is to prevent premature expression of epithelial genes that have later roles in development or function of the inner ear.

Validation of new genes regulated by FGFR2b ligands during the early stages of otocyst morphogenesis

To validate new FGFR2b target genes, we focused first on downregulated genes and assayed selected genes by ISH based on overlap in multiple RNA-Seq datasets (Table S4, sheet 5), relatively high degree of differential expression, and normalized read count above that of *Fgf3* (Table S4, sheet 1), which is difficult to detect by ISH, and, finally, novelty with respect to inner ear development and/or FGF/MAPK signaling. Seven genes validated as downregulated in RNA-Seq1 otocysts are illustrated in Fig. 7. *Spred3* was expressed in E10.25 control otocysts in a ventromedial domain, *Six2* was detected in the ventral-most region as well as laterally, and *Prdm1* (also known as *Blimp1*) was expressed similarly to *Six2* (Fig. 7A–C). All three were strongly downregulated in the corresponding experimental otocysts (Fig. 7A'–C'). *Crlf1* was also expressed similarly to *Six2* in controls, but ventral expression was absent and lateral expression was downregulated in *dnFGFR2b* otocysts (Fig. 7D,D'). *Tspan15* was expressed in a broad

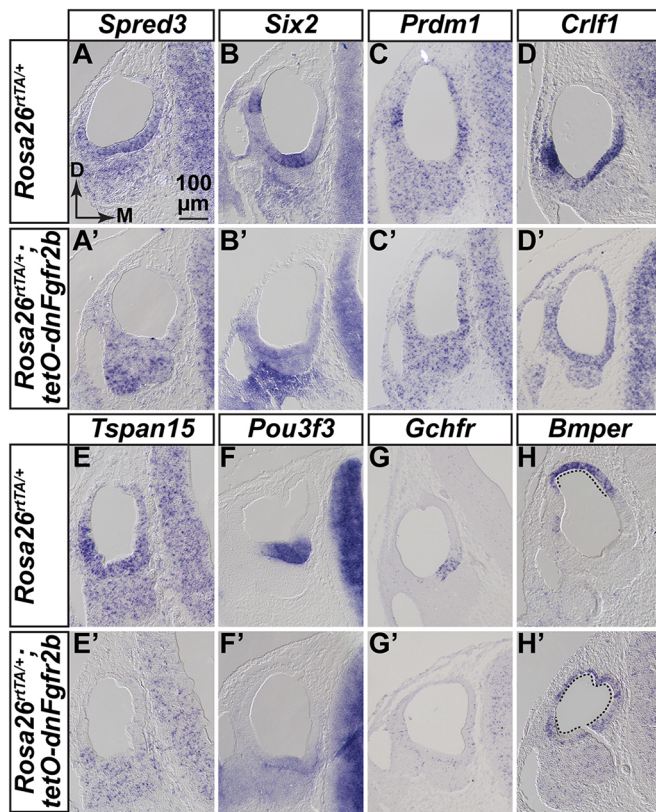


Fig. 7. Validation of new genes regulated by FGFR2b ligands during early otocyst morphogenesis. (A-H') ISH of transverse sections of E10.25 RNA-Seq1 control and *dnFgfr2b* otocysts ($n=3$ each). Probes are indicated above each column and genotypes are indicated to the left of each row. Scale and orientation for all panels is indicated in A. D, dorsal; M, medial.

ventrolateral domain in controls, whereas *Pou3f3* and *Gchfr* were expressed in the ventral-most region of controls (Fig. 7E-G) and each was absent from *dnFgfr2b* otocysts (Fig. 7E'-G'). We observed similar downregulation of *Spred3*, *Prdm1*, *Crlf1*, *Tspan15* and *Gchfr* expression in *dnFgfr2b* otocysts subjected to the Seq2 and Seq3 DOX exposures (Figs S7 and S8). *Six2* and *Pou3f3* downregulation was confirmed by ISH in Seq3 otocysts (Fig. S8), but not tested in Seq2 otocysts, as these genes were not significantly affected in the Seq2 dataset.

We also tested several genes common to the upregulated lists, but most were widely expressed in controls and any changes in expression levels were not revealed by ISH (data not shown). However, *Bmper* transcripts were confined to the dorsomedial region of control otocysts, but the expression domain expanded to encompass most of the otic epithelium in experimental otocysts (Fig. 7H,H'). Similar results obtained with Seq2 and Seq3 otocysts (Figs S7 and S8). Therefore, these datasets are a rich source of novel FGFR2b signaling targets in the early otocyst.

DISCUSSION

Fgf3 and *Fgf10* are expressed continuously throughout otocyst development

Fgf3 and *Fgf10* are likely the only relevant FGFR2b (or FGFR1b) ligand-encoding genes for early otic morphogenesis as, based on RNA-Seq data, the others are either not expressed (*Fgf22*) or are detected at negligible levels (*Fgf1* and *Fgf7*). We found that *Fgf10* has an earlier and broader distribution than *Fgf3* in the otic epithelium, and both transcripts are present in otic neuroblasts, but

Fgf3 is seen only transiently, whereas once *Fgf10* starts to be expressed, it is present continuously at high levels in the cochlear ganglion. Although *Fgf10* is expressed in mesenchyme underlying preplacodal ectoderm, neither gene appears in periotic mesenchyme during otic cup formation or later (Schimmang, 2007; Urness et al., 2015; Wright and Mansour, 2003b). ISH data for *Fgfr2b* and *Fgfr1b*, which encode the receptors for FGF3 and FGF10, are limited because of the small size of probes that distinguish them from 'c' isoforms, but extant data are consistent with the idea that they are also primarily epithelial (Orr-Urtreger et al., 1993; Pirvola et al., 2000; Wright et al., 2003; Wright and Mansour, 2003a) and, indeed, the 'b' isoforms are evident in our RNA-Seq datasets. Therefore, taken together, the ligand and receptor expression data are consistent with our findings of continuous and combinatorial roles for *Fgf3* and *Fgf10* in otic development. They also raise the interesting possibility that signaling involves epithelial and/or ganglionic ligands activating epithelial, rather than mesenchymal or ganglionic, receptors, except perhaps as neuroblasts begin delamination from the epithelium. This contrasts with the other epithelial ligands, FGF9 and FGF20, which signal canonically to mesenchymal 'c'-type receptors, inducing signals that subsequently regulate epithelial proliferation (Huh et al., 2015).

Fgf3 and *Fgf10* function continuously to promote vestibular and cochlear morphogenesis and maintenance of otic neuroblasts

Conditional mutant analyses showed that both *Fgf3* and *Fgf10* are required after otic placode induction, but deletion of *Fgf3* alone from the *Pax2-Cre* lineage was inconsequential. This contrasts with the variably penetrant otic dysmorphologies of F3KO mutants, the most severe of which initiate with alterations of dorsal otocyst patterning, loss of the EDS, and subsequent cystic development of the epithelium, ultimately resulting in hearing loss and circling behavior (Hatch et al., 2007; Mansour et al., 1993). The normal phenotype of F3cKO ears suggests a crucial role for *Fgf3* expression in the hindbrain. Indeed, we found that F10cKO embryos in which only hindbrain sources of *Fgf3* were deleted (using *Sox1^{Cre}*) had very small otocysts. In contrast, F10cKO ears had abnormalities very similar to those of F10KO ears. This demonstrates that the unique functions of *Fgf10* in otic morphogenesis arise from its expression in the placodal lineage rather than earlier in the mesenchyme. Analysis of conditional mutants that separate epithelial from ganglionic sites of *Fgf10* expression will be needed to dissect further the spatial requirements for *Fgf10* function.

Although *Pax2-Cre* is active in the placode at E8.5, we found no obvious effects at E9.5 on otocyst morphology in F3cKO;F10cKO embryos, and only two tested genes, *Etv5* and *Tbx1*, were lost or altered in these otocysts. The first major losses in expression of multiple genes required for morphogenesis occurred at E10.5. This shows that both *Fgf3* and *Fgf10* are required in the placode lineage for normal otocyst morphogenesis and suggests that overlapping expression of *Fgf3* and *Fgf10* starting at E9.5 is crucial for both cochlear and vestibular outgrowth and morphogenesis. However, the otic phenotypes of embryos with three conditionally mutant alleles point to functional differences between *Fgf3* and *Fgf10*. Both the cochlear and vestibular morphology of F3cKO; F10cHet ears was less severely affected than in F3cHet;F10cKO ears. This may reflect the larger domain and higher level of epithelial *Fgf10* than of *Fgf3*, and may be presaged by the differential effects on *Etv5* expression in the two types of E9.5 otocysts. The loss of dorsolateral *Etv5* when *Fgf10* is the only remaining allele, and of ventromedial *Etv5* when *Fgf3* is the only

remaining allele, suggest that *Fgf3* is particularly important dorsally and *Fgf10* ventrally, at least initially. The loss of dorsolateral *Tbx1* in the two most severely affected genotypes likely reflects effects of FGF3/FGF10 signaling on development of the vertical canal pouch, the derivatives of which (PSCC and ASCC) are strongly affected in these and in *Tbx1* mutants (Freyer et al., 2013; Macchiarulo and Morrow, 2017). Whether this is a direct or indirect effect on *Tbx1* expression is not yet clear, but it is interesting to note that *Tbx1* is slightly, but significantly, downregulated in the Seq2 and Seq3 datasets (Table S4, sheet 1).

The presence of an EDS in embryos with both combinations of three conditionally mutant alleles and normal *Gbx2* expression in these mutants and in F3cKO;F10cKO mutants contrasts with findings from F3KO mutants (Hatch et al., 2007), which usually lack an EDS and lose *Gbx2* expression by E10.5. This is consistent with the idea that hindbrain, rather than epithelial, *Fgf3* induces the EDS. It is possible that the further shortening of F3cHet;F10cKO CDs results from reduced FGF3-stimulated proliferation rather than alterations in molecular patterning. This is supported by preliminary analyses of E18.5 ears that did not reveal any exacerbation of changes to CD marker genes analyzed previously in the F10KO mutant (data not shown; see Urness et al., 2015). However, the timing of proliferative effects in F3cKO;F10cKO mutants must be later than E10.5, when differences in pHH3 labeling between control and F3cKO;F10cKO otocysts were not significant.

We suggested previously that *Fgf3* plays a role in otic ganglion development, as the F3KO ganglion, like that of *Fgfr2b* null mutants (Pirvola et al., 2000), appeared smaller than normal (Mansour et al., 1993). In contrast, F10KO early otic ganglia and later cochlear ganglia appear normal (Urness et al., 2015) despite defects of vestibular innervation consequent to midgestation loss of vestibular sensory epithelia (Pauley et al., 2003). In contrast to zebrafish (Vemaraju et al., 2012), our present data from F3cKO;F10cKO mutants suggest that *Fgf3* and *Fgf10* are required together for maintenance of *Neurog1* and *Neurod1* expression, and development of an otic ganglion, rather than specification of otic neuroblasts. Our data do not address whether this requirement involves ligand expression in the epithelium or ganglion or both. However, by restricting dnFGFR2b expression to the placodal lineage by using *Pax2-Cre* with the unrecombined *Rosa26^{lsrtTA}* allele, it may be possible to avoid disrupting otic induction and determine whether FGFR2b ligands play any role in mouse otic neuroblast specification. In addition, this paradigm of tissue-restricted and timed induction of dnFGFR2b could also be used to identify candidate genes responsible for neuroblast maintenance.

Temporally controlled inhibition of FGFR2b signaling during otocyst morphogenesis reveals requirements at multiple stages

Ubiquitous and sustained dnFGFR2b expression starting on different days of development revealed that FGFR2b ligands are required continuously for otic development at least until E13.5. Pulses of dnFGFR2b caused highly specific and penetrant otic malformations, supporting the idea that, unlike irreversible CRE-mediated deletion of coding exons, the signaling inhibition effected by dnFGFR2b is reversible.

Together, the sustained and pulsed inhibition paradigms suggest a distinct progression of roles for FGFR2b ligands: first in inducing the placode, then in stimulating EDS, and subsequently vestibular pouch and CD outgrowth, and finally in sculpting the SCCs, outgrowth of the utricle and saccule, and specification of CD non-sensory tissue. By comparison with genetic mutants, some

phenotypes suggest the timing of roles for FGFR2b ligands. For example, the 6–24 h period starting at E8.25 proved important for EDS formation, potentially reflecting FGF3 inhibition (Mansour et al., 1993; Hatch et al., 2007) and the 6 h period starting at E9.25 was important for PSCC formation, potentially reflecting the earliest effects of FGF10 inhibition (Pauley et al., 2003; Urness et al., 2015). Finally, inhibition from E9.75+12 h and E10.25+24 h caused phenotypes remarkably similar to those of FGF3cHet; FGF10cKO ears, suggesting a critical interval requiring both FGF3 and FGF10 for SCC maturation and CD elongation. Some vestibular phenotypes are particularly interesting as they reveal potential, but previously unsuspected, functions for FGFR2b ligands. Sustained dnFGFR2b induction starting at E10.5, or 12–24 h pulses starting at E9.75 or E10.25, blocked fusion of vestibular pouches and reduced the utricle and saccule, suggesting requirements for FGFR2b ligands in fusion plate formation and growth of the utricle and saccule. Sustained induction starting E11.5–E13.5 or 12-h pulses starting E9.75–E10.75 caused very thin SCCs, suggesting roles for FGFR2b ligands in canal pouch outgrowth and/or in limiting resorption of fusion plates. Thus, it will be interesting to explore regulatory relationships between FGFR2b signaling and genes already known to regulate vestibular morphogenesis (Alsina and Whitfield, 2017), as well as to induce dnFGFR2b in particular temporal/spatial windows and pursue unbiased identification of effector genes involved in the development of structures of interest.

FGFR2b ligands promote otic epithelial proliferation and prevent premature expression of genes required for hearing

Our RNA-Seq datasets revealed significant downregulation of genes involved in the cell cycle and DNA repair, and, indeed, immunostaining of Seq3 samples showed that mitotic cell numbers were significantly reduced in E10.25 dnFGFR2b-containing otocysts. This result differed from that obtained with E10.5 F3cKO/F10cKO otocysts, which did not show a mitotic defect. Given that hindbrain *Fgf3* is unaffected in *Pax2-Cre*;F3cKO/F10cKO mutants, and is extinguished by E10.5, it is likely that otocyst proliferation defects in these mutants would be detected at later stages of morphogenesis.

The RNA-Seq datasets also revealed significantly upregulated genes. We found that in Seq1 and Seq2, these genes are highly enriched for human hereditary hearing loss genes and mouse genes that are expressed and/or function later in the inner ear. These include *Pax2*, which was expanded in E10.5 F3cKO;F10cKO otocysts. This suggests that at early stages, FGFR2b signaling normally represses genes important for later development and function of the cochlea, or, alternatively, that the proliferative block imposed by dnFGFR2b expression promotes early differentiation of the epithelium. The latter possibility, however, does not apply to the earliest genes required for sensory cell differentiation (*Atoh1*, *Pou4f3* and *Gfi1*), which were detected at very low levels and were unaffected in any of the RNA-Seq datasets (Table S4, sheet 1). We suggest that the upregulated gene sets are worth mining for new candidates for hearing loss genes, of which many remain to be identified (Bowl and Brown, 2018).

Although we show that FGFR2b ligands are required to activate *Bmp4* and repress a BMP regulatory gene (*Bmper*), we found no evidence for FGFR2b ligand regulation of key downstream components of the BMP or SHH pathways, suggesting that although FGFR2b ligands may regulate individual components of these pathways, at least at the stages investigated, they are not exclusively upstream of these key programs directing dorsal and ventral otic morphogenesis, respectively.

Novel targets of FGFR2b signaling in early otocyst development

We validated by ISH seven novel genes downregulated and one gene upregulated by FGFR2b ligands in the RNA-seq datasets. Some genes may be regulated directly by the intracellular signaling pathway activated by FGFR2b, as one analysis point was only 12 h after induction. As we could not study more than a few differentially expressed genes, it is difficult to speculate about their combinatorial functions in inner ear development. Nevertheless, it is interesting to note that downregulated genes in our most robust dataset (Seq1) are enriched for transcription factor-coding genes (Table S4, sheet 2), including those validated here, *Six2*, *Prdm1* and *Pou3f3*. The first two have otocyst expression patterns similar to *Spred3*, *Crlf1* and *Tspan15*, whereas *Pou3f3* expression appears to overlap with *Gchfr*. This suggests that further mining of the differential expression data and generation of additional targets by employing different windows of FGFR2b inhibition, combined with promoter analysis and genome-wide studies of otocyst chromatin modification could reveal important new gene regulatory networks acting to shape the epithelium.

The only upregulated gene validated by ISH was *Bmper*, which encodes BMP-binding endothelial regulator, an ortholog of *Drosophila crossveinless 2* (*cv-2*) (Coffinier et al., 2002). *Cv-2* and *BMPER* appear to modulate BMP signaling similarly by enhancing signaling when ligands are low and limiting signaling when ligands are high (Conley et al., 2000; Dyer et al., 2014; Kelley et al., 2009; Serpe et al., 2008). Thus, *Bmper* null mutants have some phenotypes suggestive of a classic BMP signaling antagonist (Moser et al., 2003) and others suggestive of a BMP signaling agonist (Ikeya et al., 2006). Multiple BMPs and their receptors are expressed in and required for otocyst morphogenesis (Chang et al., 2008; Hwang et al., 2010; Ohyama et al., 2010) and misexpression of BMP ventral to the otic placode blocks outgrowth of the chick cochlea (Ohta et al., 2016). Thus, it will be interesting to determine whether the otic phenotype of a *Bmper* null mutant reflects a loss or gain of BMP signaling, and whether this differs in different regions. Our results also showed that at early morphogenesis stages, *Fgf3* and *Fgf10* are required for *Bmp4* expression, which is itself required for both vestibular and cochlear development (Chang et al., 2008). Determining whether FGFR2b ligand-dependent upregulation of *Bmper* functions in this context to further antagonize BMP signaling, or, alternatively, to mitigate *Bmp4* reduction by increasing signaling by other BMP ligands will require additional studies of otic *Bmp* expression and manipulation of *Bmper* levels in combination with dnFGFR2b induction at different stages.

The identification of several FGFR2b target genes not implicated previously in ear development or hearing loss syndromes provides a tantalizing glimpse into a new set of potential otocyst morphogenetic factors. Given the novelty of these targets, it is tempting to speculate that previously unappreciated regulatory pathways may be at play during otic morphogenesis, as has been postulated for otic placode induction (Anwar et al., 2017). Functional studies will be required to address the roles of each of these new genes.

MATERIALS AND METHODS

Mouse models and genotyping

Mice were maintained and euthanized in accordance with protocols approved by the University of Utah Institutional Animal Care and Use Committee. All *Fgf* mutant alleles were kept on a mixed genetic background comprised of C57BL/6 and various 129 substrains. CD-1 outbred mice (Charles River Laboratory) were used to generate embryos for studies of

normal expression patterns and for generating embryos for induction of dnFGFR2b. Noon of the day a mating plug was observed was considered E0.5. Embryos were used without regard to sex.

Generation and PCR genotyping of the *Fgf3* and *Fgf10* null alleles (*Fgf3*^{-/-}, formally designated *Fgf3*^{tm1.1Sms}=MGI:3767558, and *Fgf10*^{-/-}, formally designated *Fgf10*^{tm1.1Sms}=MGI:3526181) and *Fgf3* and *Fgf10* and conditional alleles [*Fgf3*^{cre} (*Fgf3*^{tm1.2Sms}=MGI:4456396) and *Fgf10*^{cre} (*Fgf10*^{tm1.2Sms}=MGI:4456398)] were described previously (Hatch et al., 2007; Umess et al., 2010). *Tg(Pax2-Cre)* mice [*Tg(Pax2-Cre)*1Akg=MGI:3046196] were obtained from Dr Andrew Groves (Ohshima and Groves, 2004). *Tg(Pax2-Cre)* was detected by PCR using primers specific to the transgene (5'-GGGGATCCCCGACTACAAGG-3'; 5'-TAGTGAGTCGTATTAATTTCGATAAGC-3'). The *Sox1*^{Cre} allele (Takashima et al., 2007) was transferred from Dr Mario Capecchi with permission from Dr Shin-Ichi Nishikawa (RIKEN, Japan) and genotyped using generic *Cre* primers. *Rosa26*^{lacZ} reporter mice [*Gt(ROSA)26Sor*^{tm1Sor}=MGI:1861932] (Soriano, 1999) were maintained as homozygotes.

Single conditional mutants were generated by crossing *Fgf3*^{cre/cre} females to *Fgf3*^{-/-}; *Tg(Pax2-Cre)* males or *Fgf10*^{cre/cre} females to *Fgf10*^{-/-}; *Tg(Pax2-Cre)* males. Combinations of *Fgf3* and *Fgf10* conditional mutants were obtained by crossing *Fgf3*^{cre/cre}; *Fgf10*^{cre/cre} females to *Fgf3*^{-/-}; *Fgf10*^{-/-}; *Tg(Pax2-Cre)* or for hindbrain deletion of *Fgf3* in the *Fgf10* null background, *Fgf3*^{cre/cre}; *Fgf10*^{-/-} females to *Fgf3*^{-/-}; *Fgf10*^{-/-}; *Sox1*^{Cre/+} males. *Cre* activity was confirmed by mating *Cre*-bearing males to *Rosa26*^{lacZ} females, harvesting embryos at the indicated stages and staining with X-gal as described (Yang and Mansour, 1999).

The germline-recombined *Rosa26*^{rtTA} allele [derived from *Gt(ROSA)26Sor*^{tm1(rtTA,EGFP)}Nagy; MGI:3583817] (Belteki et al., 2005; Parsa et al., 2008) and the *Tg(tetO-dnFgf2b)* allele [*Tg(tetO-Fgf2b)*1Akg=MGI:5582625] (Hokuto et al., 2003) were transferred from Dr Saverio Bellucci with permission from Dr Jeffery Whitsett (Cincinnati Children's Medical Center, OH, USA). Genotyping primers to detect *Tg(tetO-dnFgf2b)* were 5'-CAGGCCAACAGTCTGCCTGGC-3' and 5'-CGTCTGAGCTGTGTGCACCTCC-3'. *ROSA26*^{rtTA} genotyping primers were *ROSA5* (5'-GAGTCTCTGCTGCCTCCTG-3') and *ROSA3* (5'-CGAGGCGGATCACAAGCAATA-3'), which generate a wild-type band of 322 bp and *ROSA5* and *RTTA3* (5'-AAGACCGCGAAGAGTTTGTC-3'), which generate a 215 bp *rtTA*-specific product. *Rosa26*^{rtTA/+}; *Tg(tetO-dnFgf2b)* (experimental) embryos were obtained initially by crossing *Rosa26*^{rtTA/+} to *Tg(tetO-dnFgf2b)*+. For most studies described here, we crossed wild-type CD-1 females to *Rosa26*^{rtTA/rtTA}; *Tg(tetO-dnFgf2b)* males, generating 50% each of control and experimental genotypes.

RNA in situ hybridization

Embryos were harvested and fixed in 4% paraformaldehyde and stored in methanol at -20°C. RNA ISH to whole-mount embryos or paraffin-embedded sections were performed as described (Umess et al., 2008, 2010). Probes for *Sox9*, *Fgf3*, *Fgf10*, *Bmp4*, *Etv5*, *Gbx2*, *Sox2*, *Foxg1*, *Pax2*, *Neurod1*, *Neurog1* and *Crlf1* were generated by transcription of cDNA-containing plasmids. Template plasmids and acknowledgements are shown in Table S2. All other RNA probes were generated by transcription of a PCR-amplified, gene-specific 3' UTR fragment containing a T7 promoter. The primer sequences are shown in Table S3. Each panel represents the results from three independent hybridizations. Whole embryos were photographed using a stereomicroscope (Zeiss Discovery.V12) fitted with a digital camera (QImaging Micropublisher 5.0). Hybridized tissue sections were photographed under DIC illumination (Zeiss Axioskop) using a digital camera (Zeiss Axiovision or Lumenera Infinity3).

Immunostaining of frozen tissue sections for quantification of mitotic cells in the otocyst

Embryos were fixed in 4% paraformaldehyde solution and cryosectioned in the transverse plane for immunostaining as described (Umess et al., 2015). Rabbit anti-phosphohistone H3 (Millipore, 06-570) was applied at a dilution of 1:400 and mouse monoclonal anti-E-cadherin (cadherin 1) (BD Biosciences, 610181) was diluted 1:60. Rabbit anti-cleaved caspase 3

(Cell Signaling, 9661) was used at a dilution of 1:100. Secondary antibodies were from Invitrogen and diluted 1:400 into phosphate-buffered saline/0.1% Triton X-100/5% normal serum [Alexa Fluor 488 goat anti-rabbit (A11034) and Alexa Fluor 594 goat anti-mouse (A11032)]. DAPI was included in the mounting medium (Vectashield, Vector Labs). Fluorescent signals were observed under epi-illumination on a Zeiss Axioskop and captured using an Infinity3 camera (Lumenera) driven by InfinityAnalyze software. Channels were overlaid using Photoshop CS5. All pHH3-positive cells in the otocysts (defined by E-cadherin staining) were counted from 6 μm (*Pax2-Cre* cross) or 8 μm (*dnFgf2b* cross) sections extending from anterior to posterior by an individual blinded to genotype. $n=8$ control (either *Fgf3*^{-/-};*Fgf10*^{-/-} or *Fgf3*^{+/+};*Fgf10*^{+/+};*Pax2-Cre*+/+) and $n=6$ experimental (*Fgf3*^{-/-};*Fgf10*^{-/-};*Pax2-Cre*+/+) samples were counted for the *Fgf3/Fgf10/Pax2-Cre* conditional cross; $n=6$ control (*Rosa26*^{rtTA/+}) and $n=6$ experimental (*Rosa26*^{rtTA/+};*tetO-dnFgfR2b*+/+) samples for the *dnFGF2b* cross. pHH3-positive cells per ear were normalized to the cross-sectional area counted. Statistical significance was determined using an unpaired Student's *t*-test (Prism software 7.0) with Welch's correction.

Paintfilling of embryonic inner ears

Filling of embryonic inner ears with latex paint and photography was described previously (Umess et al., 2015). The number of ears with the illustrated phenotype/total ears of the same genotype is shown on each panel.

Induction of *dnFGF2b* expression

Initial inductions of *dnFGF2b* designed to phenocopy *Fgf3/Fgf10* double mutants were achieved by feeding pregnant females DOX-chow (200 mg/kg, Custom Animal Diets, LLC) *ad libitum* for the indicated time periods (E5.5-E10.5, E5.5-E11.5 or E6.5-E11.5). All subsequent inductions to generate samples for paintfilling, RNA-Seq, ISH or immunostaining were initiated by a single intraperitoneal injection of the pregnant dam with 0.1 ml/10 g body weight of 0.15 mg/ml (1.5 mg/kg body weight) doxycycline hyclate (Sigma-Aldrich) prepared in PBS followed by provision of DOX-chow *ad libitum* for the indicated time periods. We avoided using female *Rosa26*^{rtTA} parents, as these seemed to require larger and variable amounts of DOX to see phenotypes than when rtTA was contributed by the male parent, presumably because the widespread, ubiquitous expression of rtTA in females served to sequester DOX. We did not measure the time needed to reactivate signaling after DOX withdrawal, but based on studies of the limb (Danopoulos et al., 2013) we expect that signaling resumes after 12–24 h.

Otic vesicle preparation and RNA isolation

Embryos from timed matings of CD-1 females and *Rosa26*^{rtTA/rtTA};*Tg(tetO-(s)dnFgf2b)*+/+ males, with DOX exposures as specified, were dissected and the yolk sacs saved for genotyping. The otic vesicles, including surrounding mesenchyme, were crudely dissected from the head. Isolation of the vesicles free of mesenchyme was accomplished in a similar manner to methods previously described (Umess et al., 2010) with the following modifications. Otocysts with adherent mesenchyme were incubated in 50 μl ice-cold PT solution [25 mg/ml pancreatin (Sigma), 5 mg/ml trypsin (Sigma) and 5 mg/ml polyvinylpyrrolidone MW360 (Sigma) in Tyrode's solution] for ~7 min (E10.25) or ~8 min (E11.25) to promote separation of the mesenchyme. Otocysts were aspirated to Hepes-DMEM-10% fetal bovine serum, so that the digested mesenchyme could be gently teased from the underlying epithelium using fine forceps or tungsten needles, and by 'rolling' the vesicle over the bottom of the dish to detach the mesenchyme as it adhered to the plastic. The two otocysts from each embryo were aspirated into 100 μl RNeasy Lysis Buffer (Qiagen) and stored at -20°C prior to genotyping. For each of four pregnant females per DOX induction regime, all otocysts of the same genotype were combined into paired control (*Rosa26*^{rtTA/+}) and experimental [*Rosa26*^{rtTA/+};*Tg(tetO-(s)dnFgf2b)*+/+] pools ($n=6$ –12 otocysts/pool).

Total RNA from each control and experimental otocyst pool was prepared using a Micro RNAeasy kit (Qiagen, 74004) and analyzed for quantity and quality on a BioAnalyzer RNA TapeStation. All 24 samples (2 genotypes \times 4 females \times 3 DOX exposures) exceeded a RIN quality control number of 8.

RNA-Seq and bioinformatics

RNA library preparation, sequencing and analyses were conducted by the University of Utah/Huntsman Cancer Institute High-Throughput Genomics and Bioinformatic Analysis Shared Resource. Each RNA library was prepared using a TruSeq Stranded mRNA Sample Prep kit (Illumina) with oligo(dT) selection. 50-cycle single-read sequencing of each library was conducted on an Illumina Hi-Seq 2500. Sequencing reads were aligned to mm10+splice junctions (Ensembl build 74) using Novoalign (v2.08.03). Spliced alignments were converted back to genomic space, sorted and indexed using USeq (v8.8.8) SamTranscriptomeParser. Normalized coverage tracks (coverage per million mapped reads) were generated using USeq Sam2USeq and USeq2UCSCExe. Read counts for each gene were generated using USeq DefinedRegionDifferentialSeq (Nix et al., 2008) and differential expression analysis was performed using DESeq2 (Love et al., 2014) with pairing of samples from the same litters. As *Tg(tetO-dnFgf2b)* was generated from a construct in which sequences encoding the FGFR2b extracellular domain were fused to sequences encoding the hinge and Fc regions of mouse IGHG1 (Hokuto et al., 2003), elevated levels of both transgene-encoded sequences are diagnostic of successful induction in experimental tissues.

To inspect *Fgfr* splicing, we merged each set of control and *dnFgf2b* alignments to separate .bam files, uploaded them to IGV 2.4.10 (Robinson et al., 2011; Thorvaldsdottir et al., 2013) and generated Sashimi plots. To identify significantly regulated pathways ($P<0.05$, Fisher's Exact Test), all differentially expressed genes were loaded into Ingenuity Pathway Analysis (Qiagen, <https://www.qiagenbioinformatics.com/products/ingenuity-pathway-analysis/>). For gene set enrichment analysis (GSEA), two custom gene sets based on human hearing loss genes from Nishio et al. (2015) and mouse inner ear genes from Ohlemiller et al. (2016) were loaded into the Broad Institute GSEA website (Subramanian et al., 2005) and compared with ranked lists of otocyst genes sorted by fold-change from DESeq2.

Acknowledgements

We thank Katia Hatch for auditory testing of F3cKO mice, Leslie Slota for unpublished work on marker gene expression in F3cHet;F10cKO cochleae, Saverio Bellusci and Denise Al-Alam for transferring *Rosa26*^{rtTA} and *Tg(tetO-dnFgf2b)* mice, Mario Capecchi for transferring *Sox1*^{Cre} mice, Tim Mosbrugger and Chris Stubben for bioinformatics support, Shannon Odelberg for help with statistics and Gary Schoenwolf for experimental and editorial advice.

Competing interests

The authors declare no competing or financial interests.

Author contributions

Conceptualization: L.D.U., S.L.M.; Formal analysis: L.D.U., H.D., S.L.M.; Investigation: L.D.U., X.W., H.D., N.S., C.A.N., E.G.-M., R.L., S.L.M.; Writing - original draft: L.D.U., S.L.M.; Writing - review & editing: L.D.U., H.D., S.L.M.; Visualization: L.D.U., X.W., H.D., N.S., C.A.N., E.G.-M., R.L., S.L.M.; Supervision: S.L.M.; Project administration: S.L.M.; Funding acquisition: S.L.M.

Funding

This work was funded by grants from the National Institutes of Health (R01 DC011819 and R01 DC004185 to S.L.M.) and a National Science Foundation-funded SDB CHOOSE Development! Fellowship (IOS-1239422 to E.G.-M.). Deposited in PMC for release after 12 months.

Data availability

The three RNA-seq datasets are deposited in Gene Expression Omnibus under accession number GSE116404.

Supplementary information

Supplementary information available online at <http://dev.biologists.org/lookup/doi/10.1242/dev.170142.supplemental>

References

Al Alam, D., El Agha, E., Sakurai, R., Kheirollahi, V., Moiseenko, A., Danopoulos, S., Shrestha, A., Schmoldt, C., Quantius, J., Herold, S. et al. (2015). Evidence for the involvement of fibroblast growth factor 10 in lipofibroblast formation during embryonic lung development. *Development* **142**, 4139–4150.

- Alsina, B. and Whitfield, T. T.** (2017). Sculpting the labyrinth: morphogenesis of the developing inner ear. *Semin. Cell Dev. Biol.* **65**, 47-59.
- Alvarez, Y., Alonso, M. T., Vendrell, V., Zelarayan, L. C., Chamero, P., Theil, T., Bösl, M. R., Kato, S., Maconochie, M., Riethmacher, D. et al.** (2003). Requirements for FGF3 and FGF10 during inner ear formation. *Development* **130**, 6329-6338.
- Anwar, M., Tambalo, M., Ranganathan, R., Grocott, T. and Streit, A.** (2017). A gene network regulated by FGF signalling during ear development. *Sci. Rep.* **7**, 6162.
- Basch, M. L., Brown, R. M., II, Jen, H.-I. and Groves, A. K.** (2016). Where hearing starts: the development of the mammalian cochlea. *J. Anat.* **228**, 233-254.
- Belteki, G., Haigh, J., Kabacs, N., Haigh, K., Sison, K., Costantini, F., Whitsett, J., Quaggin, S. E. and Nagy, A.** (2005). Conditional and inducible transgene expression in mice through the combinatorial use of Cre-mediated recombination and tetracycline induction. *Nucleic Acids Res.* **33**, e51.
- Bowl, M. R. and Brown, S. D. M.** (2018). Genetic landscape of auditory dysfunction. *Hum. Mol. Genet.* **27**, R130-R135.
- Chang, W., Brigande, J. V., Fekete, D. M. and Wu, D. K.** (2004). The development of semicircular canals in the inner ear: role of FGFs in sensory cristae. *Development* **131**, 4201-4211.
- Chang, W., Lin, Z., Kulesha, H., Hebert, J., Hogan, B. L. M. and Wu, D. K.** (2008). Bmp4 is essential for the formation of the vestibular apparatus that detects angular head movements. *PLoS Genet.* **4**, e1000050.
- Chi, C. L., Martinez, S., Wurst, W. and Martin, G. R.** (2003). The isthmus organizer signal FGF8 is required for cell survival in the prospective midbrain and cerebellum. *Development* **130**, 2633-2644.
- Coffinier, C., Ketpura, N., Tran, U., Geissert, D. and De Robertis, E. M.** (2002). Mouse *Crossveinless-2* is the vertebrate homolog of a *Drosophila* extracellular regulator of BMP signaling. *Mech. Dev.* **119** Suppl. 1, S179-S184.
- Conley, C. A., Silburn, R., Singer, M. A., Ralston, A., Rohwer-Nutter, D., Olson, D. J., Gelbart, W. and Blair, S. S.** (2000). *Crossveinless 2* contains cysteine-rich domains and is required for high levels of BMP-like activity during the formation of the cross veins in *Drosophila*. *Development* **127**, 3947-3959.
- Danopoulos, S., Parsa, S., Al Alam, D., Tabatabai, R., Baptista, S., Tiozzo, C., Carraro, G., Wheeler, M., Barreto, G., Braun, T. et al.** (2013). Transient inhibition of FGFR2b-ligands signaling leads to irreversible loss of cellular beta-catenin organization and signaling in AER during mouse limb development. *PLoS ONE* **8**, e76248.
- Dyer, L., Wu, Y., Moser, M. and Patterson, C.** (2014). BMPER-induced BMP signaling promotes coronary artery remodeling. *Dev. Biol.* **386**, 385-394.
- Freyer, L., Nowotschin, S., Pirity, M. K., Baldini, A. and Morrow, B. E.** (2013). Conditional and constitutive expression of a Tbx1-GFP fusion protein in mice. *BMC Dev. Biol.* **13**, 33.
- Hatch, E. P., Noyes, C. A., Wang, X., Wright, T. J. and Mansour, S. L.** (2007). Fgf3 is required for dorsal patterning and morphogenesis of the inner ear epithelium. *Development* **134**, 3615-3625.
- Hokuto, I., Perl, A.-K. T. and Whitsett, J. A.** (2003). Prenatal, but not postnatal, inhibition of fibroblast growth factor receptor signaling causes emphysema. *J. Biol. Chem.* **278**, 415-421.
- Huh, S.-H., Warchol, M. E. and Ornitz, D. M.** (2015). Cochlear progenitor number is controlled through mesenchymal FGF receptor signaling. *eLife* **4**, e05921.
- Hwang, C. H., Guo, D., Harris, M. A., Howard, O., Mishina, Y., Gan, L., Harris, S. E. and Wu, D. K.** (2010). Role of bone morphogenetic proteins on cochlear hair cell formation: analyses of *Noggin* and *Bmp2* mutant mice. *Dev. Dyn.* **239**, 505-513.
- Ikeya, M., Kawada, M., Kiyonari, H., Sasai, N., Nakao, K., Furuta, Y. and Sasai, Y.** (2006). Essential pro-Bmp roles of *crossveinless 2* in mouse organogenesis. *Development* **133**, 4463-4473.
- Isaiah, A., Lee, D., Lenes-Voit, F., Sweeney, M., Kutz, W., Isaacson, B., Roland, P. and Lee, K. H.** (2017). Clinical outcomes following cochlear implantation in children with inner ear anomalies. *Int. J. Pediatr. Otorhinolaryngol.* **93**, 1-6.
- Kelley, R., Ren, R., Pi, X., Wu, Y., Moreno, I., Willis, M., Moser, M., Ross, M., Podkowa, M., Attisano, L. et al.** (2009). A concentration-dependent endocytic trap and sink mechanism converts Bmp6 from an activator to an inhibitor of Bmp signaling. *J. Cell Biol.* **184**, 597-609.
- Kimura, Y., Masuda, T. and Kaga, K.** (2018). Vestibular function and gross motor development in 195 children with congenital hearing loss-assessment of inner ear malformations. *Otol. Neurotol.* **39**, 196-205.
- Ladher, R. K.** (2017). Changing shape and shaping change: inducing the inner ear. *Semin. Cell Dev. Biol.* **65**, 39-46.
- Ladher, R. K., Wright, T. J., Moon, A. M., Mansour, S. L. and Schoenwolf, G. C.** (2005). FGF8 initiates inner ear induction in chick and mouse. *Genes Dev.* **19**, 603-613.
- Lin, Z., Cantos, R., Patente, M. and Wu, D. K.** (2005). Gbx2 is required for the morphogenesis of the mouse inner ear: a downstream candidate of hindbrain signaling. *Development* **132**, 2309-2318.
- Love, M. I., Huber, W. and Anders, S.** (2014). Moderated estimation of fold change and dispersion for RNA-seq data with DESeq2. *Genome Biol.* **15**, 550.
- Macchiarulo, S. and Morrow, B. E.** (2017). Tbx1 and Jag1 act in concert to modulate the fate of neurosensory cells of the mouse otic vesicle. *Biol. Open* **6**, 1472-1482.
- Mansour, S. L., Goddard, J. M. and Capecechi, M. R.** (1993). Mice homozygous for a targeted disruption of the proto-oncogene *int-2* have developmental defects in the tail and inner ear. *Development* **117**, 13-28.
- Morsli, H., Choo, D., Ryan, A., Johnson, R. and Wu, D. K.** (1998). Development of the mouse inner ear and origin of its sensory organs. *J. Neurosci.* **18**, 3327-3335.
- Moser, M., Binder, O., Wu, Y., Aitsebaomo, J., Ren, R., Bode, C., Bautch, V. L., Conlon, F. L. and Patterson, C.** (2003). BMPER, a novel endothelial cell precursor-derived protein, antagonizes bone morphogenetic protein signaling and endothelial cell differentiation. *Mol. Cell Biol.* **23**, 5664-5679.
- Nishio, S. Y., Hattori, M., Moteki, H., Tsukada, K., Miyagawa, M., Naito, T., Yoshimura, H., Iwasa, Y., Mori, K., Shima, Y. et al.** (2015). Gene expression profiles of the cochlea and vestibular endorgans: localization and function of genes causing deafness. *Ann. Otol. Rhinol. Laryngol.* **124** Suppl. 1, 6s-48s.
- Nix, D. A., Courdy, S. J. and Boucher, K. M.** (2008). Empirical methods for controlling false positives and estimating confidence in ChIP-Seq peaks. *BMC Bioinformatics* **9**, 523.
- Ohlemiller, K. K., Jones, S. M. and Johnson, K. R.** (2016). Application of Mouse Models to Research in Hearing and Balance. *J. Assoc. Res. Otolaryngol.* **17**, 493-523.
- Ohta, S. and Schoenwolf, G. C.** (2018). Hearing crosstalk: the molecular conversation orchestrating inner ear dorsoventral patterning. *Wiley Interdiscip. Rev. Dev. Biol.* **7**, e302.
- Ohta, S., Wang, B., Mansour, S. L. and Schoenwolf, G. C.** (2016). BMP regulates regional gene expression in the dorsal otocyst through canonical and non-canonical intracellular pathways. *Development* **143**, 2228-2237.
- Ohyama, T. and Groves, A. K.** (2004). Generation of Pax2-Cre mice by modification of a Pax2 bacterial artificial chromosome. *Genesis* **38**, 195-199.
- Ohyama, T., Basch, M. L., Mishina, Y., Lyons, K. M., Segil, N. and Groves, A. K.** (2010). BMP signaling is necessary for patterning the sensory and nonsensory regions of the developing mammalian cochlea. *J. Neurosci.* **30**, 15044-15051.
- Orr-Urtreger, A., Bedford, M. T., Burakova, T., Arman, E., Zimmer, Y., Yayon, A., Givol, D. and Lonai, P.** (1993). Developmental localization of the splicing alternatives of fibroblast growth factor receptor-2 (FGFR2). *Dev. Biol.* **158**, 475-486.
- Parsa, S., Ramasamy, S. K., De Langhe, S., Gupta, V. V., Haigh, J. J., Medina, D. and Bellusci, S.** (2008). Terminal end bud maintenance in mammary gland is dependent upon FGFR2b signaling. *Dev. Biol.* **317**, 121-131.
- Parsa, S., Kuremoto, K., Seidel, K., Tabatabai, R., Mackenzie, B., Yamaza, T., Akiyama, K., Branch, J., Koh, C. J., Al Alam, D. et al.** (2010). Signaling by FGFR2b controls the regenerative capacity of adult mouse incisors. *Development* **137**, 3743-3752.
- Pauley, S., Wright, T. J., Pirvola, U., Ornitz, D., Beisel, K. and Fritzsche, B.** (2003). Expression and function of FGF10 in mammalian inner ear development. *Dev. Dyn.* **227**, 203-215.
- Pirvola, U., Spencer-Dene, B., Xing-Qun, L., Kettunen, P., Thesleff, I., Fritzsche, B., Dickson, C. and Ylikoski, J.** (2000). FGF/FGFR-2(IIIb) signaling is essential for inner ear morphogenesis. *J. Neurosci.* **20**, 6125-6134.
- Pirvola, U., Zhang, X., Mantela, J., Ornitz, D. M. and Ylikoski, J.** (2004). Fgf9 signaling regulates inner ear morphogenesis through epithelial-mesenchymal interactions. *Dev. Biol.* **273**, 350-360.
- Robinson, J. T., Thorvaldsdóttir, H., Winckler, W., Guttman, M., Lander, E. S., Getz, G. and Mesirov, J. P.** (2011). Integrative genomics viewer. *Nat. Biotechnol.* **29**, 24-26.
- Sajan, S. A., Warchol, M. E. and Lovett, M.** (2007). Toward a systems biology of mouse inner ear organogenesis: gene expression pathways, patterns and network analysis. *Genetics* **177**, 631-653.
- Sato, T. and Joyner, A. L.** (2009). The duration of Fgf8 isthmus organizer expression is key to patterning different tectal-isthmus-cerebellum structures. *Development* **136**, 3617-3626.
- Schimmang, T.** (2007). Expression and functions of FGF ligands during early otic development. *Int. J. Dev. Biol.* **51**, 473-481.
- Sennaroglu, L. and Bajin, M. D.** (2017). Classification and current management of inner ear malformations. *Balkan. Med. J.* **34**, 397-411.
- Serpe, M., Umulis, D., Ralston, A., Chen, J., Olson, D. J., Avanesov, A., Othmer, H., O'Connor, M. B. and Blair, S. S.** (2008). The BMP-binding protein *Crossveinless 2* is a short-range, concentration-dependent, biphasic modulator of BMP signaling in *Drosophila*. *Dev. Cell* **14**, 940-953.
- Soriano, P.** (1999). Generalized lacZ expression with the ROSA26 Cre reporter strain. *Nat. Genet.* **21**, 70-71.
- Subramanian, A., Tamayo, P., Mootha, V. K., Mukherjee, S., Ebert, B. L., Gillette, M. A., Paulovich, A., Pomeroy, S. L., Golub, T. R., Lander, E. S. et al.** (2005). Gene set enrichment analysis: a knowledge-based approach for interpreting genome-wide expression profiles. *Proc. Natl. Acad. Sci. USA* **102**, 15545-15550.
- Takahima, Y., Era, T., Nakao, K., Kondo, S., Kasuga, M., Smith, A. G. and Nishikawa, S.-I.** (2007). Neuroepithelial cells supply an initial transient wave of MSC differentiation. *Cell* **129**, 1377-1388.

- Thorvaldsdottir, H., Robinson, J. T. and Mesirov, J. P.** (2013). Integrative Genomics Viewer (IGV): high-performance genomics data visualization and exploration. *Brief. Bioinform.* **14**, 178-192.
- Urness, L. D., Li, C., Wang, X. and Mansour, S. L.** (2008). Expression of ERK signaling inhibitors Dusp6, Dusp7, and Dusp9 during mouse ear development. *Dev. Dyn.* **237**, 163-169.
- Urness, L. D., Paxton, C. N., Wang, X., Schoenwolf, G. C. and Mansour, S. L.** (2010). FGF signaling regulates otic placode induction and refinement by controlling both ectodermal target genes and hindbrain Wnt8a. *Dev. Biol.* **340**, 595-604.
- Urness, L. D., Wang, X., Shibata, S., Ohyama, T. and Mansour, S. L.** (2015). Fgf10 is required for specification of non-sensory regions of the cochlear epithelium. *Dev. Biol.* **400**, 59-71.
- Vemaraju, S., Kantarci, H., Padanad, M. S. and Riley, B. B.** (2012). A spatial and temporal gradient of Fgf differentially regulates distinct stages of neural development in the zebrafish inner ear. *PLoS Genet.* **8**, e1003068.
- Whitfield, T. T.** (2015). Development of the inner ear. *Curr. Opin. Genet. Dev.* **32**, 112-118.
- Wright, T. J. and Mansour, S. L.** (2003a). Fgf3 and Fgf10 are required for mouse otic placode induction. *Development* **130**, 3379-3390.
- Wright, T. J. and Mansour, S. L.** (2003b). FGF signaling in ear development and innervation. *Curr. Top. Dev. Biol.* **57**, 225-259.
- Wright, T. J., Hatch, E. P., Karabagli, H., Karabagli, P., Schoenwolf, G. C. and Mansour, S. L.** (2003). Expression of mouse fibroblast growth factor and fibroblast growth factor receptor genes during early inner ear development. *Dev. Dyn.* **228**, 267-272.
- Wu, D. K. and Kelley, M. W.** (2012). Molecular mechanisms of inner ear development. *Cold Spring Harb. Perspect. Biol.* **4**, a008409.
- Xu, J., Liu, Z. and Ornitz, D. M.** (2000). Temporal and spatial gradients of Fgf8 and Fgf17 regulate proliferation and differentiation of midline cerebellar structures. *Development* **127**, 1833-1843.
- Yang, W. and Mansour, S. L.** (1999). Expression and genetic analysis of prtb, a gene that encodes a highly conserved proline-rich protein expressed in the brain. *Dev. Dyn.* **215**, 108-116.
- Zelarayan, L. C., Vendrell, V., Alvarez, Y., Domínguez-Frutos, E., Theil, T., Alonso, M. T., Maconochie, M. and Schimmang, T.** (2007). Differential requirements for FGF3, FGF8 and FGF10 during inner ear development. *Dev. Biol.* **308**, 379-391.
- Zhang, X., Ibrahimi, O. A., Olsen, S. K., Umemori, H., Mohammadi, M. and Ornitz, D. M.** (2006). Receptor specificity of the fibroblast growth factor family. The complete mammalian FGF family. *J. Biol. Chem.* **281**, 15694-15700.

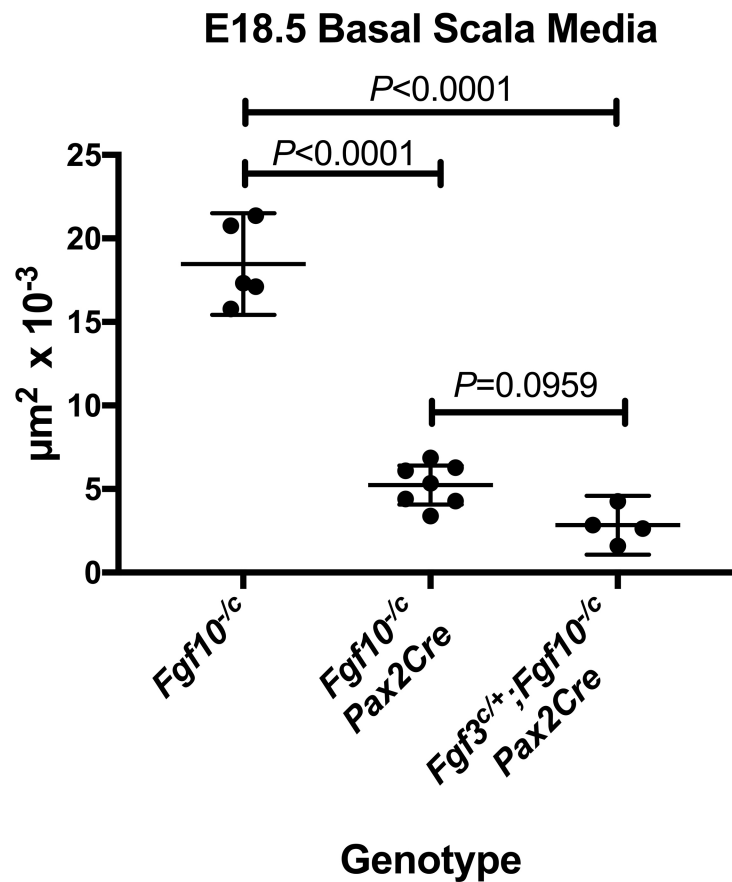


Figure S1. Removing one copy of *Fgf3* from the F10cKO background does not significantly affect the area of the scala media. Scala media area (μm^2) was determined for three genotypes, *Fgf10*^{-/-} (controls, n=5, not shown in Fig. 2), *Fgf10*^{-/-}; *Pax2-Cre*/+ (F10CKO, n=6; Fig. 2G) and *Fgf3*^{c/+}; *Fgf10*^{-/-}; *Pax2-Cre*/+ (F3cHet;F10CKO, n=4; Fig. 2R). Mean and 95% confidence intervals are indicated. One-way ANOVA with Tukey's multiple comparisons test was used to calculate significance.

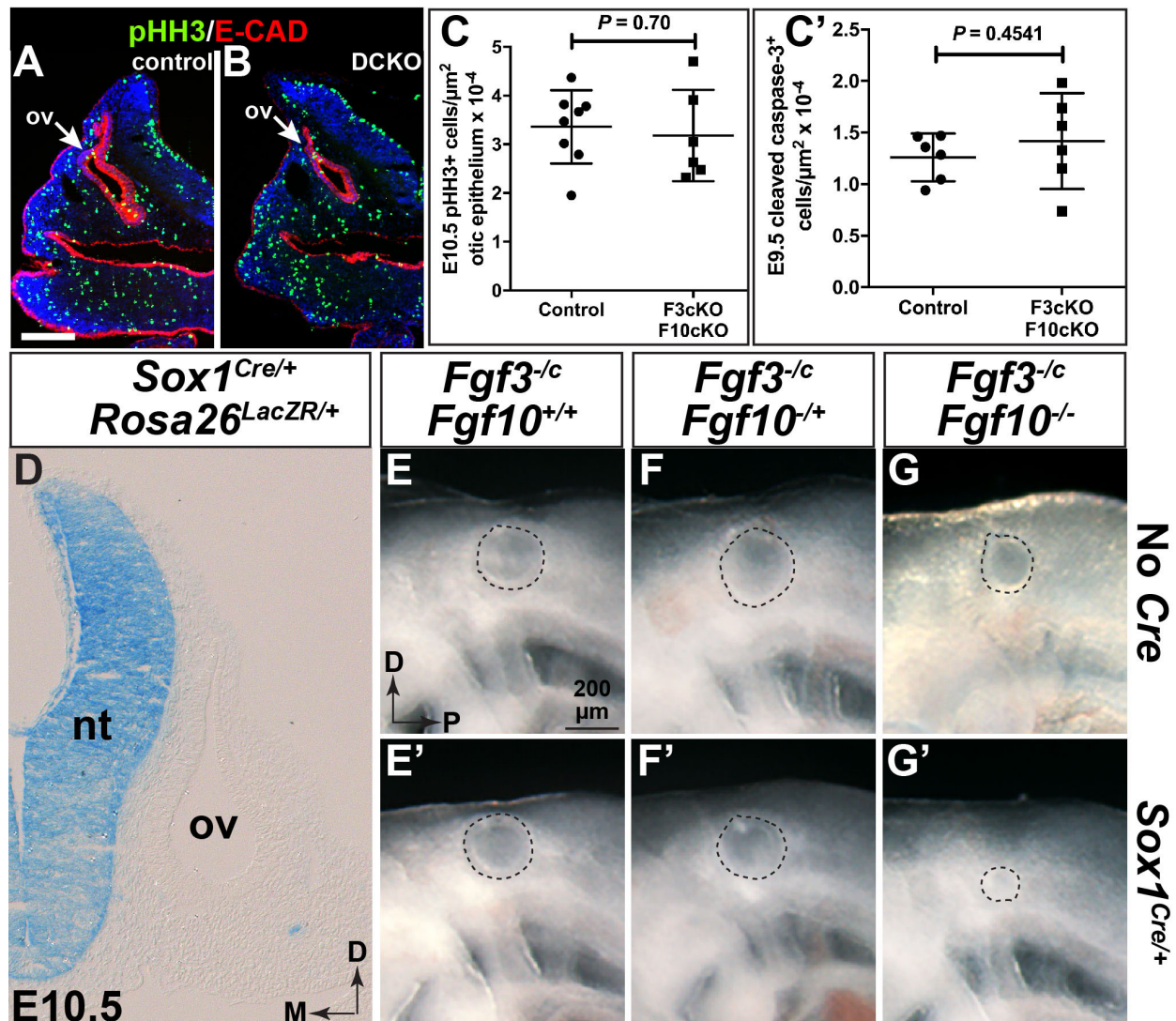


Figure S2. *Fgf3* and *Fgf10* are not required in the *Pax2-Cre* lineage for early otocyst proliferation or survival, likely because *Fgf3* expression persists in the hindbrain, where it is required for development of a normally sized otic vesicle. (A,B) Transverse cryosections of E10.5 control (*Fgf3*^{-/-};*Fgf10*^{-/-}) and double conditional mutant (DCKO; *Fgf3*^{-/-};*Fgf10*^{-/-};Tg(*Pax2-Cre*)/+) otic vesicles (ov) immunostained to detect pHH3 (green) and E-Cadherin (red). Scale bar in A (100 μm) applies to B. (C) Quantification of pHH3-positive cells per otic epithelial area shows no significant difference between genotypes. (C') Quantification of cleaved-caspase-3 cells per otic epithelial area shows no significant difference between genotypes at E9.5. (D) Transverse section at the level of the otic vesicle of an E10.5 X-gal-stained *Rosa26*^{LacZR/+};*Sox1*^{Cre/+} embryo shows CRE activity restricted to the neural tube. (E-G') Lateral views of otic vesicles from freshly dissected E9.5 embryos show that in the global absence of *Fgf10*, hindbrain *Fgf3* is required to develop a normally sized otic vesicle (G'). *Fgf* genotypes are indicated above and *Cre* status is to the right of each row. Dashed lines denote the external circumference of the otic epithelium. The scale bar and orientation axes in E apply to E-G'. Abbreviations: D, dorsal; M, medial, nt, neural tube; ov, otic vesicle; P, posterior.

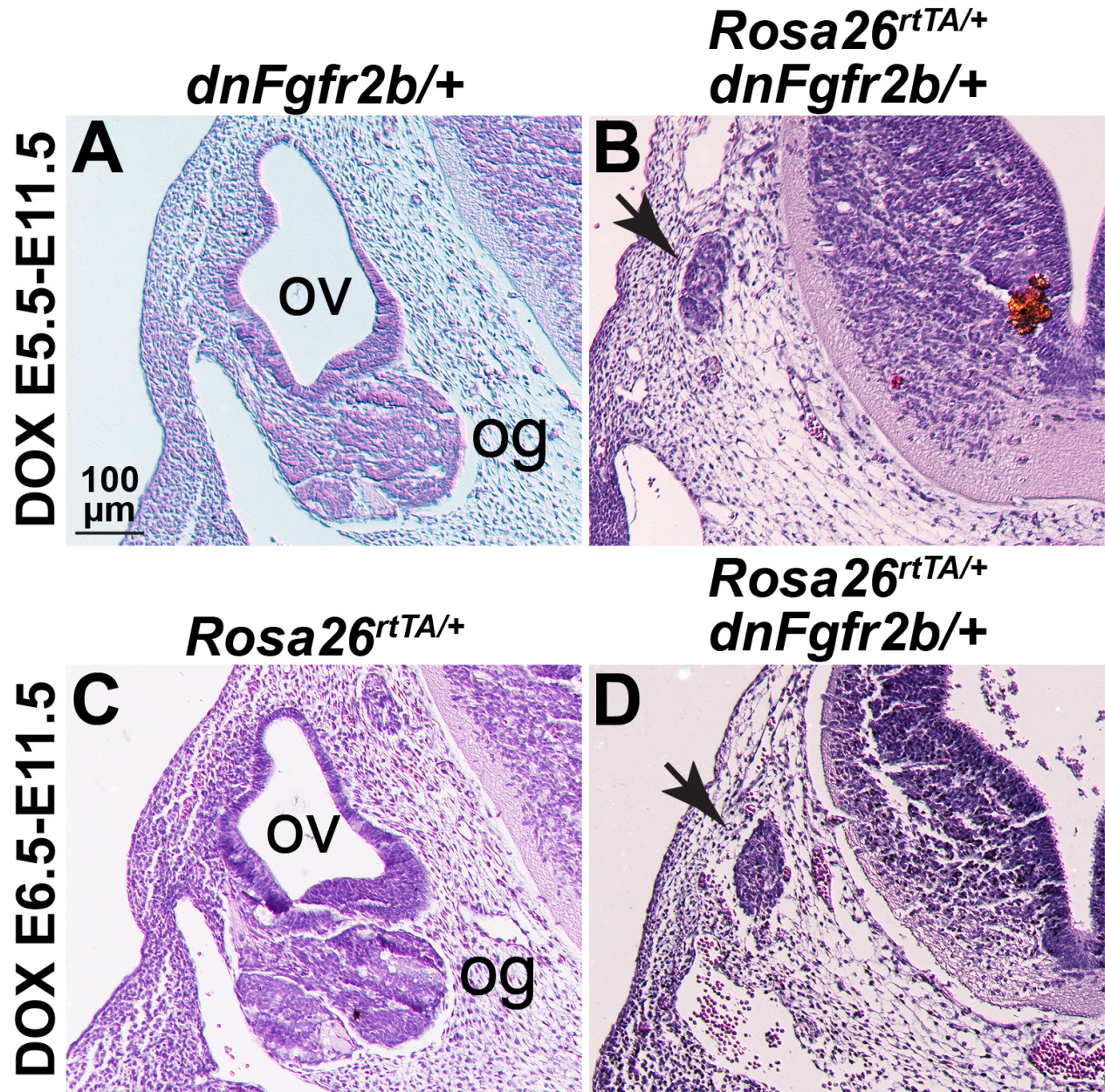


Figure S3. Induction of dnFGFR2b prior to otic placode induction blocks otic vesicle formation. Transverse hematoxylin and eosin-stained sections of embryos derived from *Tg(tetO-dnFgfr2b)/+* females crossed to *Rosa26^{rtTA/+}* males and fed DOX-chow between E5.5-E11.5 (A,B) or E6.5-E11.5 (C,D). Genotypes are indicated above each column and DOX induction conditions indicated to the left of each row. Remnant otic tissue in the experimental samples is indicated with an arrow (B,D). The scale bar in A applies to all panels. Abbreviations: og, otic ganglion; ov, otic vesicle.

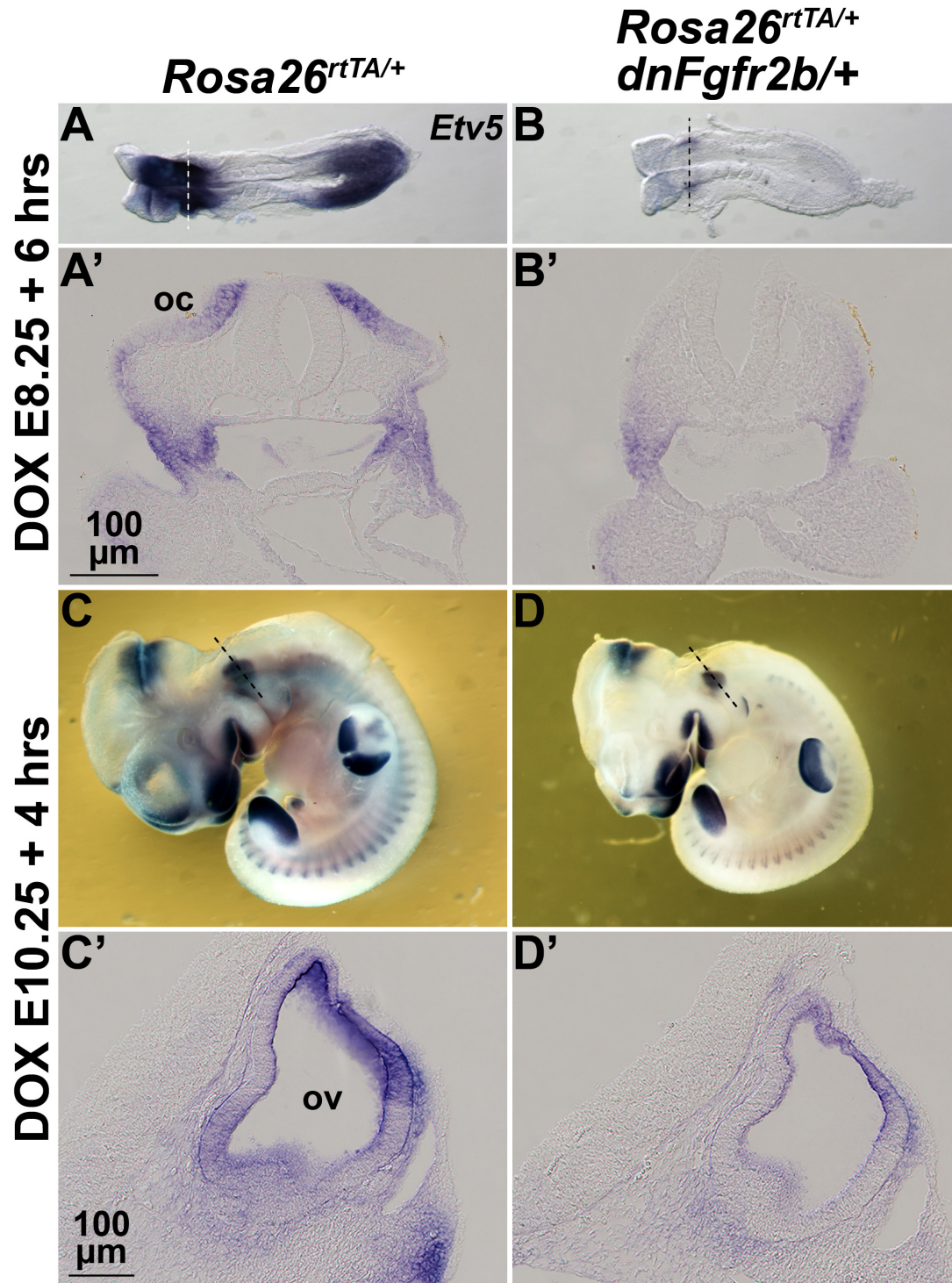


Figure S4. Inhibition of FGFR2b ligands has a rapid onset. Whole-mount ISH with an *Etv5* probe on embryos derived from wild type females crossed to *Rosa26^{rtTA/rtTA};Tg(*tetO-dnFgfr2b*)/+* males and treated with DOX for six hours beginning at E8.25 (A-B') or 4 hours beginning at E10.5 (C-D'). Genotypes are indicated above each column. Dashed lines (A,B,C,D) indicate the planes of transverse sections shown in A',B',C',D'. Abbreviations: oc, otic cup; ov, otic vesicle.

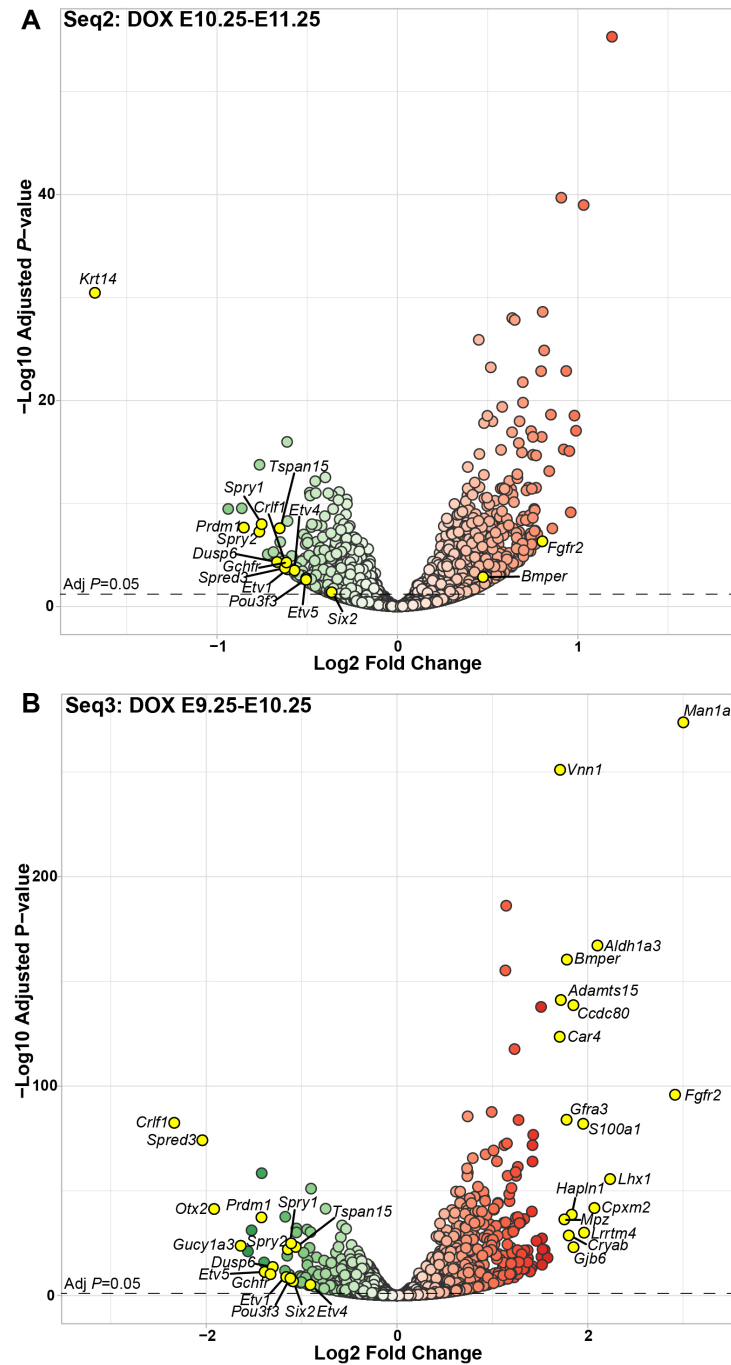


Figure S5. Differential RNA-Seq analysis of otic epithelia subjected to overlapping and longer dnFGFR2b induction windows define a stage-specific FGFR2b signaling response during early otic morphogenesis. (A) Volcano plot of the RNA-Seq2 (DOX exposure E10.25-E11.25), and (B) RNA-Seq3 (DOX exposure from E9.25-E10.25) datasets. Down-regulated (green) and up-regulated (red) genes were identified using a paired statistical model (see Methods). The statistical significance of the differential expression is shown on the y-axis and the fold change is shown on the x-axis. Names for genes highlighted in yellow include all those with a fold-change > 1.5, plus known FGF target genes and genes that we pursued for expression validation.

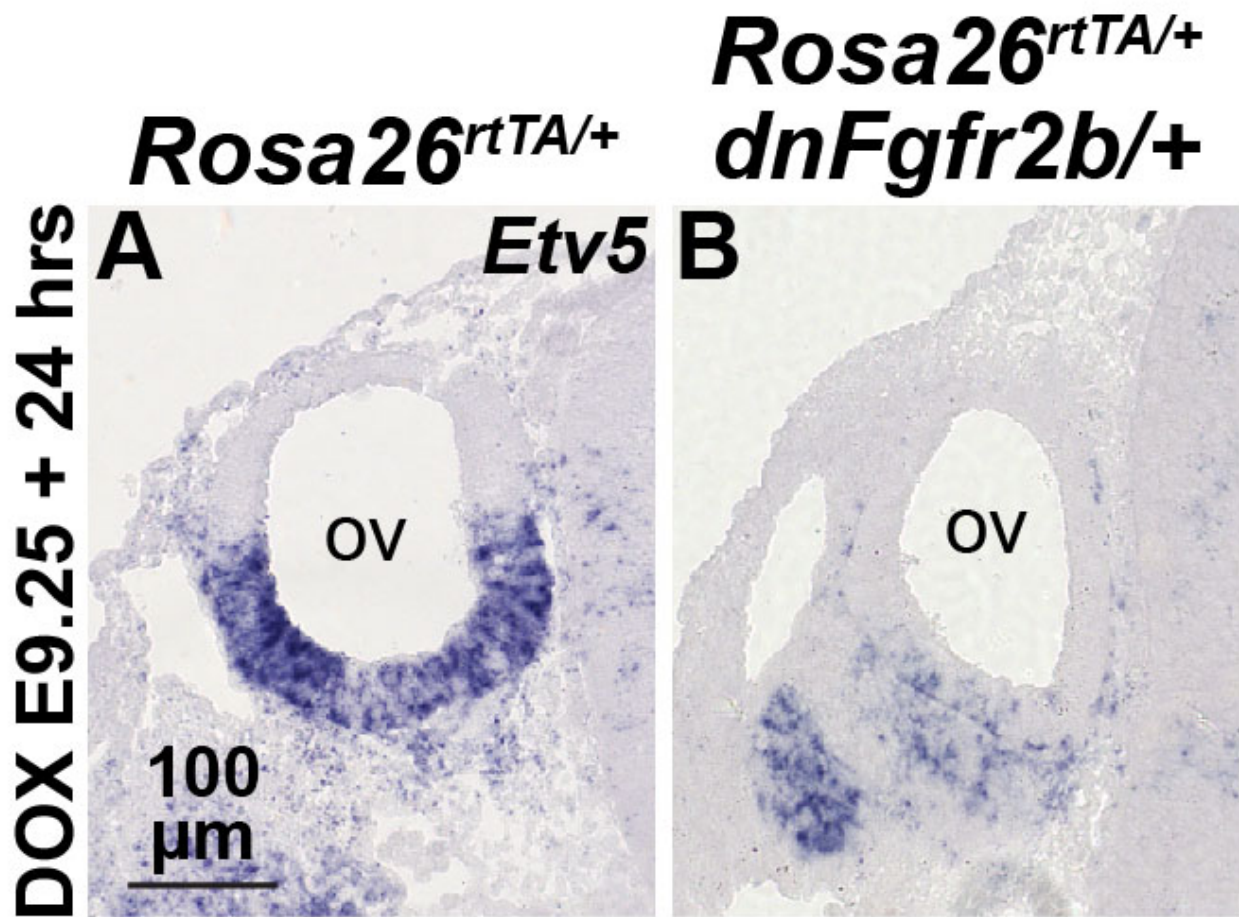


Figure S6. *Etv5* is lost from the otic vesicle following RNA-Seq3 dnFGFR2b induction conditions. ISH using an *Etv5* probe on sections taken through the otic vesicle (ov) and ganglion (og) from control (A) (*Rosa26^{rtTA/+}*) or *dnFgfr2b*-expressing embryos (B) subjected to Seq3 induction conditions (E9.25-E10.25, n=3 each).

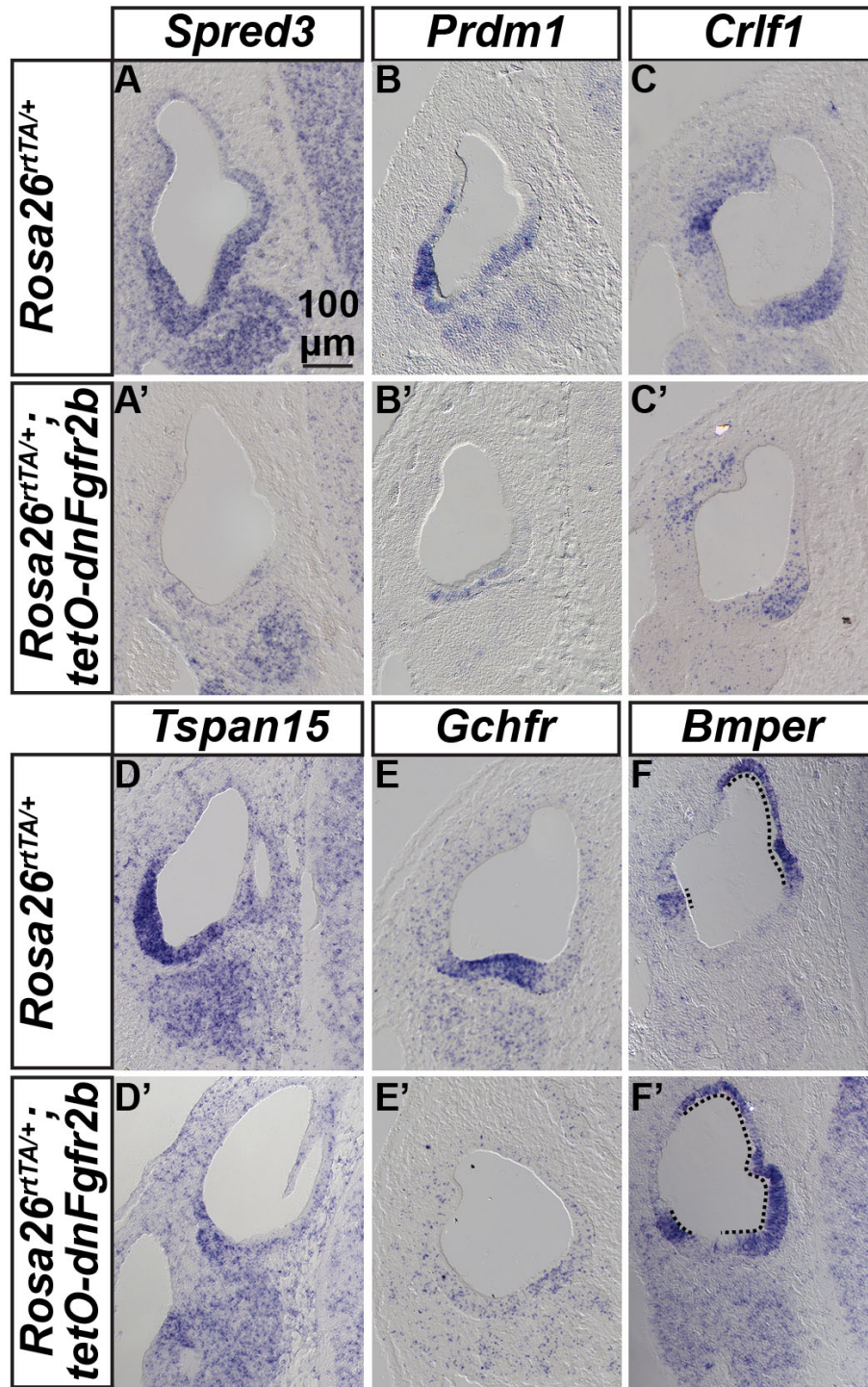


Figure S7. Validation of the subset of new FGFR2b ligand-dependent genes differentially expressed under RNA-Seq2 induction conditions. ISH of transverse E11.25 paraffin sections of otocysts exposed to Seq2 induction conditions (DOX, E10.25-E11.25). Probes are indicated in the boxes above each column and genotypes are indicated to the left of each row (controls A-F, dnFGFR2b-expressing embryos A'-F', n=3 each). Dorsal is up, medial is to the right. The scale bar in A applies to all panels. The dotted line in F and F' demarks *Bmper* expression.

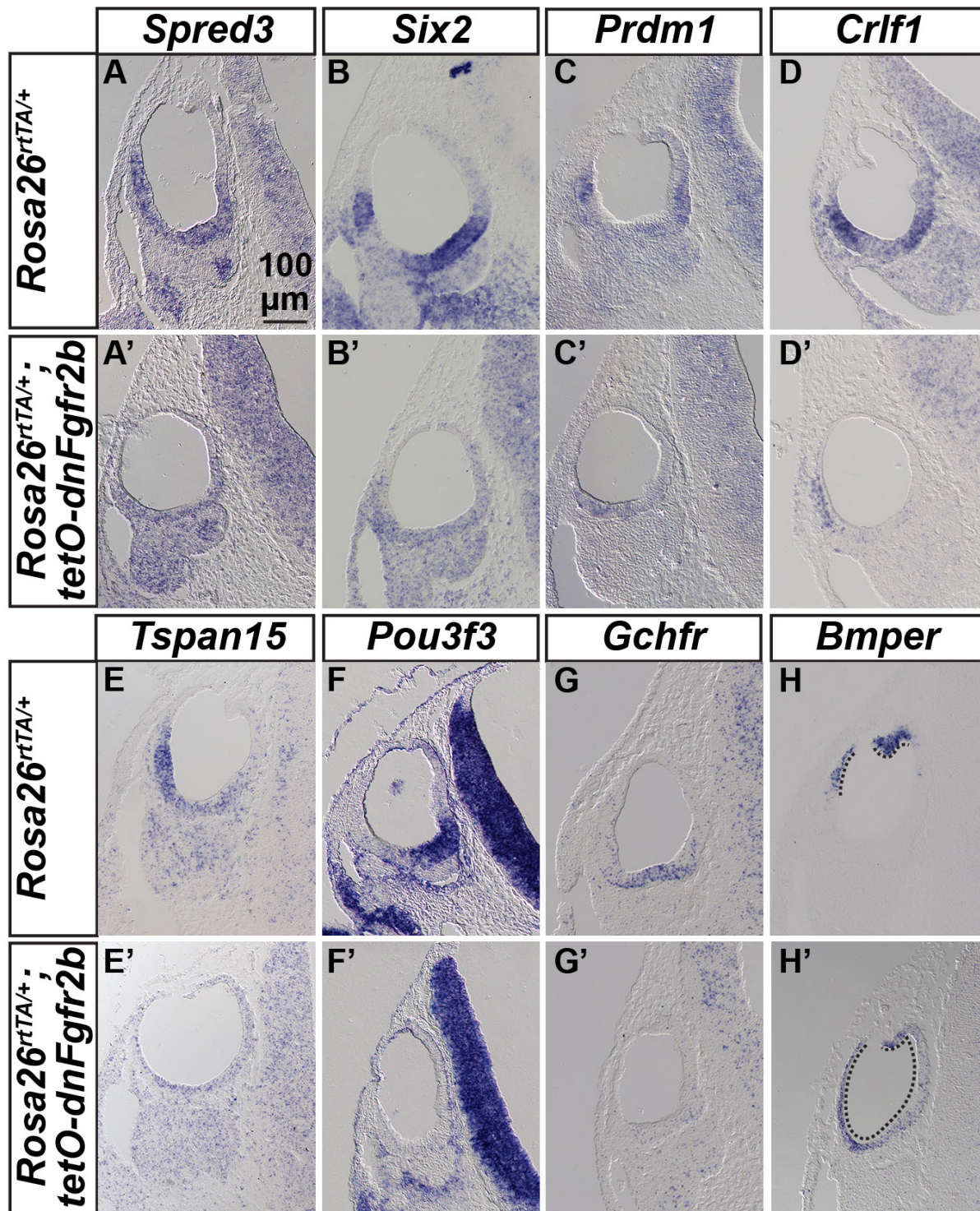


Figure S8. Validation of the subset of new FGFR2b ligand-dependent genes differentially expressed under RNA-Seq3 induction conditions. ISH of transverse E10.25 paraffin sections of otocysts exposed to Seq3 induction conditions (DOX, E9.25-E10.25). Probes are indicated in the boxes above each column and genotypes are indicated to the left of each row (controls A-H, dnFGFR2b-expressing embryos A'-H', n=3 each). Dorsal is up, medial is to the right. The scale bar in A applies to all panels. The dotted line in H and H' demarks *Bmper* expression.

Table S1

Phenotypes resulting from loss of epithelial *Fgf3* and *Fgf10* alleles in the Tg(*Pax2-Cre*) lineage

CRE negative	<i>Fgf3</i> ^{-/-}	<i>Fgf10</i> ^{-/-}	<i>Fgf3</i> ^{C/+} ; <i>Fgf10</i> ^{C/+}	<i>Fgf3</i> ^{-/-} ; <i>Fgf10</i> ^{C/+}	<i>Fgf3</i> ^{C/+} ; <i>Fgf10</i> ^{-/-}	<i>Fgf3</i> ^{-/-} ; <i>Fgf10</i> ^{-/-}
C0	4	0	10	3	0	0
C1	0	4	1	9	6	0
C2	0	3	0	0	6	6
C3	0	0	0	0	2	0
C4	0	0	0	0	0	0
C5	0	0	0	0	0	0
CRE positive	<i>Fgf3</i> ^{-/-}	<i>Fgf10</i> ^{-/-}	<i>Fgf3</i> ^{C/+} ; <i>Fgf10</i> ^{C/+}	<i>Fgf3</i> ^{-/-} ; <i>Fgf10</i> ^{C/+}	<i>Fgf3</i> ^{C/+} ; <i>Fgf10</i> ^{-/-}	<i>Fgf3</i> ^{-/-} ; <i>Fgf10</i> ^{-/-}
C0	8	0	0	0	0	0
C1	0	2	9	3	0	0
C2	0	8	3	11	0	0
C3	0	6	0	0	2	0
C4	0	0	0	0	13	0
C5	0	0	0	0	2	16

Gross phenotypic classes

C0=normal morphology

C1=reduced PSSC, normal cochlea

C2=absent PSSC, normal cochlea

C3=absent PSSC/variable lsc and ascc, short cochlea

C4=unfused vertical canal pouches, shortened cochlea

C5=spheroid chamber lacking distinct vestibule or cochlea

Scoring of paintfill phenotypic classes by *Fgf* genotype and *Pax2-Cre* status. C0-C4 were defined previously by Urness et al. (2015) for *Fgf10* heterozygous and homozygous germline mutants. C5, the most severe class, was never observed in *Fgf10* germline mutants. The most prevalent phenotype for each genotype is indicated in bold; examples of the most prevalent phenotypes are shown in Figure 2L-O'. The distribution of phenotypes is significantly different between the F10cKO and F3cHet;F10cKO ears ($P < 0.0001$; Fisher's exact test; SPSS software).

Table S2**cDNA clones used to prepare digoxigenin-labeled cRNA antisense transcripts for in situ hybridization**

Gene	Insert size (bp)	Enzyme (antisense)	Polymerase	Source	Reference
<i>Bmp4</i>	~900	AccI	T7	Anne Boulet	Jones et al., 1991
<i>Sox9</i>	~400	EcoRI	T3	Anne Boulet	Wright et al., 1995
<i>Fgf3</i>	373	BamHI	T3	Nancy Manley	Wright and Mansour, 2003
<i>Fgf10</i>	~550	EcoRI	SP6	David Ornitz	Xu et al., 1998
<i>Etv5</i>	458	EcoRI	T7	GenBank NM_023794 Residues 1309-1766	Li et al., 2007
<i>Gbx2</i>	~1000	HindIII	T7	Gail Martin	Wassarman et al., 1997
<i>Sox2</i>	530	HindIII	T7	Olivia Bermingham-McDonogh	Wood and Episkopou, 1999
<i>Foxg1</i>	~400	HindIII	T7	GenBank A1592649 Residues 2615-2976	Pauley et al., 2006
<i>Pax2</i>	~500	BamHI	T3	Peter Gruss	Dressler et al., 1990
<i>Neurod1</i>	~1500	EcoRI	T3	Gary Gaufo	Liu et al., 2000
<i>Neurog1</i> (hydrolyzed)	~2000	XhoI	T7	Quifu Ma	Ma et al., 2000

Purified plasmid DNA was digested with the indicated restriction enzyme and then transcribed with the indicated RNA polymerase to produce antisense probes for ISH.

Table S3**Primers used to generate DNA fragments for cRNA probe generation.**

Gene	Primers	Primer sequences (5'-3')	Product size (bp)
<i>Spred3</i>	F-916	TTCTACCGTTCACTGGGATTCC	~675
	R-915	CCAAACCAGCTCAACAATCC	
<i>Six2</i>	F-936	AGTTCCGAGGATGAGAAGACG	~510
	R-937	CTTGCCTAGTTCAAGACTCGG	
<i>Prdm1</i>	F-908	ATCCATCTCTGCAGCCTCAAGG	~490
	R-907	GCAGATCTGGAGTCATGTACAAGC	
<i>Tspan15</i>	F-968	TACTGTACATCACCCGTGTGG	~625
	R-969	AGCCTTACAGAGGACTCAAGG	
<i>Pou3f3</i>	F-925	GGGACATCTCGTTTATACTGTGG	~745
	R-926	TGTCTTTCCACACCCTTTTATCGG	
<i>Gchfr</i>	F-939	ACGAATACTACGTCAACGACC	~460
	R-940	GAACAACCACTTGTGAGAGCC	
<i>Bmper</i>	F-970	GTGATAACTGGAATGAGATCGG	~670
	R-971	GTGAAATCTGACAGACTCTCCTTGG	
<i>Crlf1</i> *	F-946	AGCAGTCAGGAGACAATCTGG	~620
	R-947	AACGCACTTGGACAAGTAAACGG	

Forward (F) and reverse (R) primers used to PCR-amplify 3'UTR regions of each indicated gene from mouse genomic DNA, except *Crlf1*, which was amplified from a cDNA clone. All reverse primers include the T7 promoter sequence (GGATCCTAATACGACTCACTATAGGGAG) at the 5' end. The antisense-RNA strand was produced by transcription of the PCR product using T7 RNA polymerase. *Crlf1* cDNA 3 from DNASU Arizona State University Clone # MmCD00295268 (NCBI NM_018827.2, Image: 100063851).

Table S4.**Sheet 1: Fgfs, Fgfrs, targets**

Compilation of normalized mean control and experimental count values from DSeq2 paired analyses for *Fgfs*, *Fgfrs* and select target genes with corresponding log2FoldChange and adjusted *P*-values (padj) from the RNA-Seq1, -Seq2 and -Seq3 datasets. Ensembl mouse gene numbers are shown (col A) if the gene was detected in at least one of the datasets. Gene names (col B) follow mouse conventions. Log2FoldChange cells are shaded in red to indicate significant upregulation and in green to indicate significant downregulation, roughly corresponding to the scheme used in the volcano plots. Padj values were derived following the Benjamini-Hochberg multiple testing correction. NA in the padj column indicates that there were outlier counts present in one or more groups.

Sheet 2: IPA,GO_paired top 5 path

Output of Ingenuity Pathway and GOrilla analyses. Rows 3-21 Ingenuity Pathway Analysis (IPA) output for the top 5 regulated pathways in each RNA-seq dataset. The cutoff for differential expression *P*-value in each dataset was 0.05. There was no cutoff for fold-change. Column heading definitions are shown on the sheet. Rows 35-61. GOrilla process analysis output for downregulated genes with an adjusted *P*-value of <0.05 and no fold-change cutoff in RNA-Seq1-3 paired datasets and GOrilla function analysis for downregulated genes in RNA-Seq1 with a Max AdjP-value <0.05 and log2(fold-change) >0.585. (<http://cbl-gorilla.cs.technion.ac.il/>) Column heading definitions are shown on the sheet.

Sheet 3: Seq1 GSEA_AORL,NISHIO

Gene set enrichment analysis (GSEA) of all 16232 RNA-Seq1 genes ranked by fold-change, using 93 human hearing loss genes listed in Nishio et al. (2015) (<https://software.broadinstitute.org/gsea/doc/GSEAUUserGuideFrame.html>), including the enrichment table (cols A-H) and plot. GSEA column heading and plot definitions are shown on the sheet.

Sheet 4: Seq1 GSEA_JAX

Gene set enrichment analysis (GSEA) of all 16232 RNA-Seq1 genes ranked by fold-change, using 258 mouse inner ear-associated genes listed in Ohlemiller et al. (2016) (<https://software.broadinstitute.org/gsea/doc/GSEAUUserGuideFrame.html>) including the enrichment table (cols A-H) and plot. GSEA column heading and plot definitions are shown on the sheet.

Sheet 5: intersect datasets

Intersections of downregulated and upregulated RNA-Seq1-3 gene lists with corresponding Venn diagrams generated using GeneVenn software (<http://genevenn.sourceforge.net/>). Downregulated genes with an AdjP <0.05 and FC>1.5 were overlapped separately from upregulated genes with an AdjP <0.01 and FC> 2. Gene lists comprising overlap in all three sets and for each pair are shown. Annotations of the gene lists are shown on the sheet.

[Click here to Download Table S4](#)